Master Erasmus Mundus in Photonics Engineering, Nanophotonics and Biophotonics

Europhotonics

MASTER THESIS WORK

Shortcuts to adiabaticity for the transport of matter waves

Abdullah Rasmita

Supervised by
Dr. Jordi Mompart, Dr. Veronica Ahufinger
(Universitat Autònoma de Barcelona , UAB)
Dr. Heinz Kalt
(Karlsruhe Institute of Technology, KIT)

Presented in Barcelona, on September 10th, 2013

Registered at

Escola Tècnica Superior d'Enginyeria de Telecomunicació de Barcelona

TABLE OF CONTENTS

ABSTRACT

In this master thesis we investigate the quantum transport of a single neutral atom in double-well and triple-well potentials. In particular, we study and implement the Fast-Forward technique to speed up the quantum dynamics of the Three-Level Atom Optics (TLAO) based transport. We show that the resulting technique is faster and, against certain experimental imperfections, more robust than the usual TLAO-based transport. Moreover, we address different shortcuts to adiabaticity examples. First, we derive a more general shortcut to adiabaticity for adiabatic translation than the one reported in the literature. Also, we obtain a criterion for the realization of a shortcut to adiabaticity and we show that, under this criterion, it is impossible to derive a realizable shortcut to adiabaticity using the Fast-Forward technique for the TLAO-based transport.

ACKNOWLEDGEMENTS

The author would like to express his appreciation to all people who have helped him in completing this project. It is impossible to mention them one by one in this very limited space.

The author was introduced to the topic of this project by his project supervisors at Universitat Autònoma de Barcelona (UAB), Dr. Jordi Mompart and Dr. Veronica Ahufinger. Their inputs for some problems encountered by the author in this project have played a key role in the completion of this project. Their effort in reviewing this report is very much appreciated. For all of these, the author would like to offer his gratitude.

The part of this report related to Spatial Light Modulator is, partly, a result of the author's discussion with Mr. Alex Turpin. The author would like to thank him for this and for being such a helpful colleague. The author would also like to thank Dr. Heinz Kalt of Karlsruher Institut für Technologie (KIT) for his willingness to be the KIT supervisor for this project.

This project is part of the Europhotonics master program. The author has been very fortunate to have been granted with the Erasmus Mundus scholarship to participate in this program. The author would like to thank the European Union for this invaluable opportunity.

Lastly, but certainly not least, the author would like to thank his parents for their support. They are one of the main sources of motivation for the author to keep studying and, hopefully one day, to become a more useful human being.

CHAPTER ONE
Introduction

1.1. Background and motivation

As the technology follows the trend of utilizing smaller and smaller objects, we will reach a point where manipulation of objects as tiny as single atoms will be unavoidable. This need of controlling single atoms is matched with the development of experimental tools to manipulate them [1,2].

One case that has increasingly become more important is the control of the transport of a single atom. High fidelity transport of a single atom can be done by adiabatically moving the potential where it is trapped in or by using other means such as the tunneling-based transport [3] and the Three-Level Atom Optics (TLAO) based transport [4]. In the tunneling-based transport, the atom is transported between the two traps of a double-well potential while in the TLAO-based transport, it is transported between the two extreme traps of a triple-well potential. These two techniques have been shown to be useful in the field of quantum information [3, 4].

The drawback of an adiabatic transport is that it is too slow. In recent years, some techniques have been proposed to accelerate adiabatic processes, that is to create a shortcut to adiabaticity [5,6]. Among many of these techniques are the transitionless tracking algorithm [7], the inverse engineering of external driving based on Lewis-Riesenfeld invariants [6], optimal control methods [8], the parallel adiabatic passage [9], and the Fast-Forward technique [10]. As mentioned in [5], experimental realizations of some of these procedures have been reported.

In this project, our main focus is the Fast-Forward technique [10,11]. In this technique, the quantum dynamics of a process is accelerated by adding an additional phase to the wave function. One of the advantages of the Fast-Forward technique is that, in terms of programming, one Fast-Forward program can be applied to a wide range of problems by only changing some of the parameters. Some examples of the numerical implementation of this technique have been reported in the literature. Among them are fast-forwarding of adiabatic translation, wave packet splitting, wave packet squeezing, and acceleration of quantum dynamics in electromagnetic fields [10,12].

Up to the author's knowledge, the Fast-Forward technique has not been applied to the TLAO-based transport. Also, there has not been any shortcut to adiabaticity based on the Fast-Forward technique or any other techniques that has been designed specifically for the TLAO-based transport. However, it is worth mentioning that a shortcut to adiabaticity for the population transfer in three-level systems has been derived using invariant-based inverse engineering in [13]. Though it was suggested in [13] that the shortcut to adiabaticity described there can also be applied to the transport of atoms in a triple well, it was not shown how this could be done. There is also work done on speeding up the TLAO-based transport by using optimal control [14].

1.2. Objective and scope

Our main focus in this project is the implementation of the Fast-Forward technique to accelerate the TLAO-based transport of a single neutral atom between two extreme traps of a triple-well potential. We limit our discussion to piecewise harmonic potentials. Numerical simulations are conducted to check the validity of the results.

1.3. Outline

In Chapter 2, we provide a review of the quantum dynamics of a single neutral atom in a single, double-well and triple-well harmonic potential focusing especially on the the transport issue. The tunneling-based transport in a double-well potential [3] is described. For the case of the triple-well potential, the technique discussed is based on the Three-Level Atom Optics (TLAO) concept [4]. The advantages and drawbacks of each transport technique are highlighted.

In Chapter 3, we give the description and the derivation of the Fast-Forward technique [11] and the shortcut to adiabaticity based on this technique [10]. We discuss two examples of the implementation of this technique. The first one is its implementation to accelerate the adiabatic translation of a single neutral atom in a potential well. For this first example, we follow a different derivation than the one given in [10]. By doing so, we obtain a more general result. The second example corresponds to the speeding up of the TLAO-based transport.

The conclusions of this master thesis are given in Chapter 4. In this last chapter, we also give some suggestions on possible future research directions related to the subject presented in this master thesis.

CHAPTER TWO
Transport of a single neutral atom

In this chapter, we start with a review of the quantum harmonic oscillator and then discuss more involved systems such as the double-well and the triple-well potentials. The main focus will be the description of the schemes to transport a single neutral atom between the two traps of a double-well harmonic potential and the two extreme traps of a triple-well harmonic potential, respectively. As we will see later in this chapter, while the use of a triple-well potential allows for a more robust transport, it has a drawback that the process is slower compared to the case where a double-well potential is used.

Throughout this report, letters *x* and *t* represent space and time variables, respectively, except if it is specified otherwise. We consider time-dependent and time-independent one dimensional (1D) Schrödinger equations with the following forms

$$i\hbar\frac{\partial}{\partial t}\Psi(x,t)=\hat{H}\Psi(x,t) \tag{2.1a}$$

$$E\,\Phi(x)=\hat{H}\Phi(x), \tag{2.1b}$$

respectively, where $\hat{H}=\frac{-\hbar^2}{2m}\frac{\partial^2}{\partial x^2}+V(x,t)$ is the Hamiltonian of the system and *V(x,t)* is the spatial and temporal-dependent potential. The normalization condition, $|\Psi(x,t)|=|\Phi(x)|=1$ and initial condition $\Psi(x,0)=\Psi_0(x)$ are applied.

2.1. Quantum harmonic oscillator

Quantum harmonic oscillator can refer to different physical systems which have similar form of the Hamiltonian. In our case, it refers to a system where a single neutral atom is trapped in a harmonic potential. There are two reasons for examining this system:

1. This system has an analytical solution. Hence, it can be used to test our simulation program (see Appendix A for the description of the simulation program).
2. Near an equilibrium point, most physical potentials can be modeled as a harmonic oscillator.

The potential function for a harmonic trap can be written as

$$V(x)=\frac{\hbar\omega}{2L^2}x^2, \tag{2.2}$$

where ω is the angular frequency of the harmonic trap, and *L* is the oscillation length defined by $L=\sqrt{\frac{\hbar}{m\omega}}$ with *m* being the mass of the atom.

The eigenstates (eigenfunctions) and eigenvalues of (2.1b) for the quantum harmonic oscillator case are well known and can be expressed as

$$\Phi_n(x)=\frac{\pi^{-1/4}}{\sqrt{L}}\frac{1}{\sqrt{(2^n n!)}}e^{\frac{-x^2}{2L^2}}H_n(\frac{x}{L}), \tag{2.3a}$$

$$E_n=(n+\frac{1}{2})\hbar\omega, \tag{2.3b}$$

respectively. Here, $H_n(u)$ is the Hermite polynomial of degree n. Note that the eigenfunctions are either odd or even functions. In fact, it is easy to prove that the eigenfunctions of any non-degenerate Hamiltonian with a real symmetric potential are either odd or even functions. This will be important when studying the double-well potential in the next section.

We obtained the eigenfunctions and energy eigenvalues corresponding to the ground state and the first three excited states numerically using the Imaginary Time Propagation method (see the detail in Appendix A). The results of the numerical simulation are shown in Figure 1(a-d). Note that only the real part of the wave function is shown. This is because the analytical solution is completely real and the imaginary part obtained in the simulation is negligible. From these figures, we can see that the simulation results strongly agree with equation (2.3a).

The following energy eigenvalues (in units of $\hbar\omega$) are also obtained from the simulation:

$$E_0 = 0.4997, E_1 = 1.4984, E_2 = 2.4959, E_3 = 3.4922 .$$

As can be seen, the obtained eigenvalues are in strong agreement with the analytical eigenvalues given in equation (2.3b). Another observation is that the agreement between the simulated eigenvalues and equation (2.3b) is worse for the higher excited states. This is because the eigenfunctions for the higher excited states are broader than those for the lower ones. Hence, to get the same accuracy, a larger computational domain is needed.

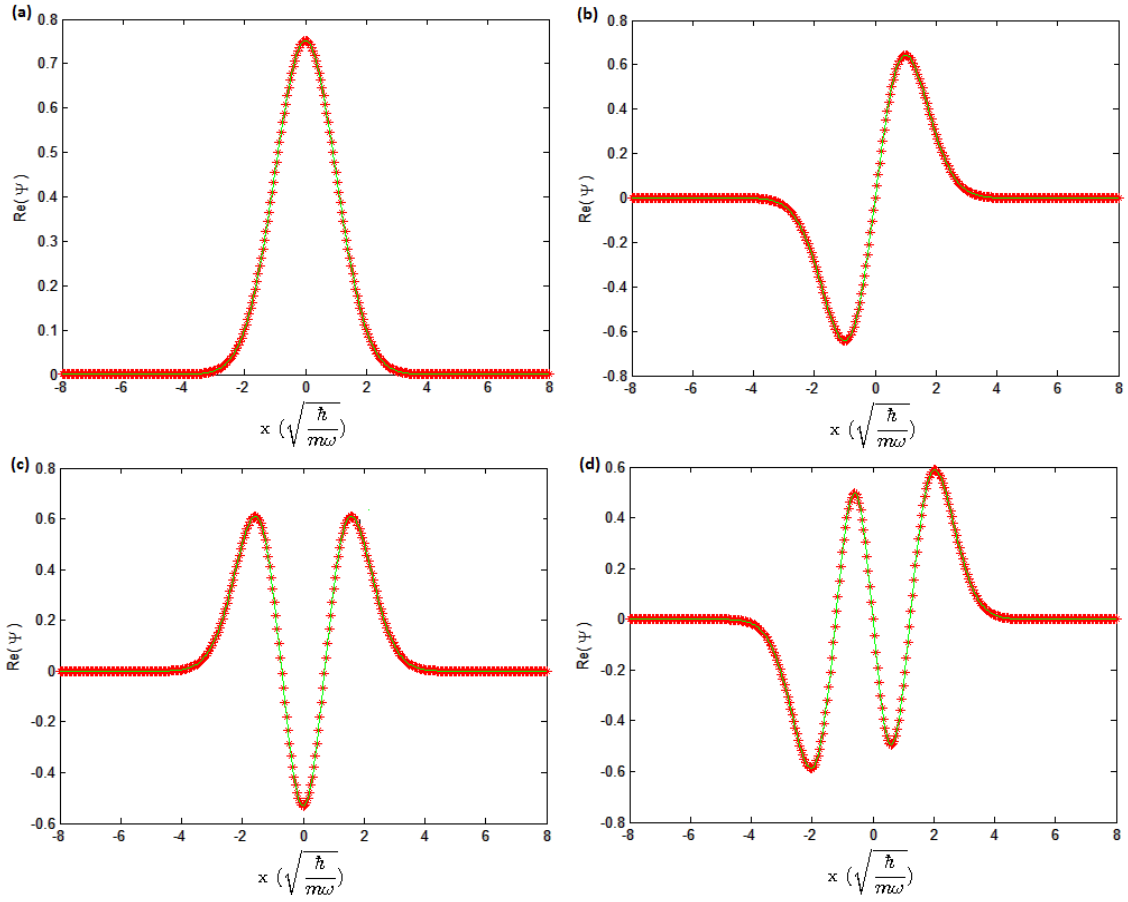

Figure 1. Real part of the eigenfunctions of the ground state (a), and the first three excited states (b,c,d) of a quantum harmonic oscillator. The red dots (*) represent the simulation results while the green lines (——) represent the analytical solutions.

In order to test our simulation program for the time dependent Schrödinger equation, let us consider the solution of (2.1a),

$$\Psi(x,t)=\sum_{(n=0)}^{\infty}\Phi_n(x)\int \mathrm{d}\,x\,\Phi_n^*(x)\Psi(x,0)e^{\frac{-iE_n t}{\hbar}}. \qquad (2.4)$$

We apply equation (2.4) for the case of the quantum harmonic oscillator case. For this case, $\Phi_n(x)$ and E_n are given by (2.3a) and (2.3b), respectively. By inserting (2.3a) and (2.3b) into (2.4), we can see that, for the quantum harmonic oscillator, the wave function, $\Psi(x,t)$, has an oscillation period, $T_s \le \frac{4\pi}{\omega}$, and the probability density, $P_d(x,t)=\Psi^*(x,t)\Psi(x,t)$ has an oscillation period, $T_p \le \frac{2\pi}{\omega}$.

We consider two types of oscillation

1. Breathing mode

   Consider a case where the wave function at the initial time is a narrowed version of the ground state's eigenfunction. In other words, $\Psi(x,0)=\Phi_0(kx)$ with $k > 1$. In this case, $P_d(x,t)$ is a Gaussian function with its width oscillating with a period of $\frac{\pi}{\omega}$. The reason it is $\frac{\pi}{\omega}$ and not $\frac{2\pi}{\omega}$ is because the wave function is an even function so any odd eigenfunction will not contribute to the wave function. This makes the oscillation two times faster.

2. Dipole oscillation

   In this second case, the wave function at the initial time is the ground state's eigenfunction shifted by Δx in space. In other words, $\Psi(x,0)=\Phi_0(x-\Delta x)$. In this case, $P_d(x,t)$ is a Gaussian wave packet oscillating around the origin with a period equal to $\frac{2\pi}{\omega}$. The amplitude of the oscillation is equal to Δx.

The results of our simulation for both cases are shown in Figure 2(a-b). Figure 2a shows the contour plot, in time and space, of the probability density for the case of breathing and Figure 2b shows this contour plot for the case of dipole oscillation. It can be seen that both breathing and dipole oscillation are simulated correctly. The oscillation period for the breathing is $\sim\pi$ and for the dipole oscillation is $\sim 2\pi$, both are in units of $\frac{1}{\omega}$. This is in full agreement with the discussion above.

Based on the comparison between the simulation results and the analytical solutions, we can conclude that our simulation programs for both the time dependent and time independent Schrödinger equations are accurate.

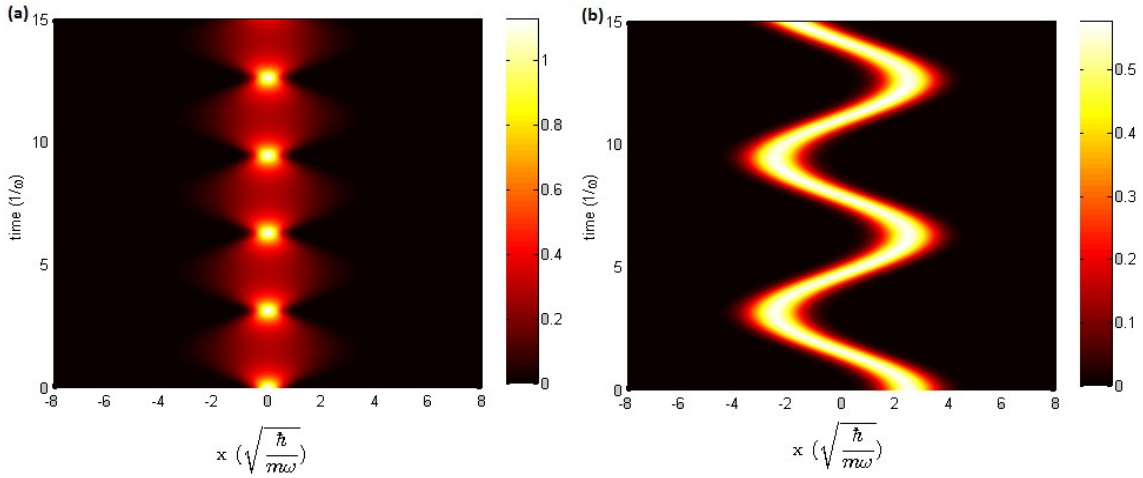

Figure 2. Probability density of a single neutral atom in a harmonic potential in the case of (a) breathing with $k = 2$ and (b) dipole oscillation with $\Delta x = 2.5\,L$.

2.2. Double-well potential

Next, we consider a single neutral atom in a double-well potential. We consider the following piecewise harmonic potential

$$V(x,t) = \begin{matrix} \frac{\hbar\omega}{2L^2}(x+d)^2, x<0 \\ \frac{\hbar\omega}{2L^2}(x-d)^2, x\geq 0 \end{matrix} \qquad (2.5)$$

where the separation distance between the center of each of the two wells is equal to 2*d*. Figure 3 illustrates the shape of this potential.

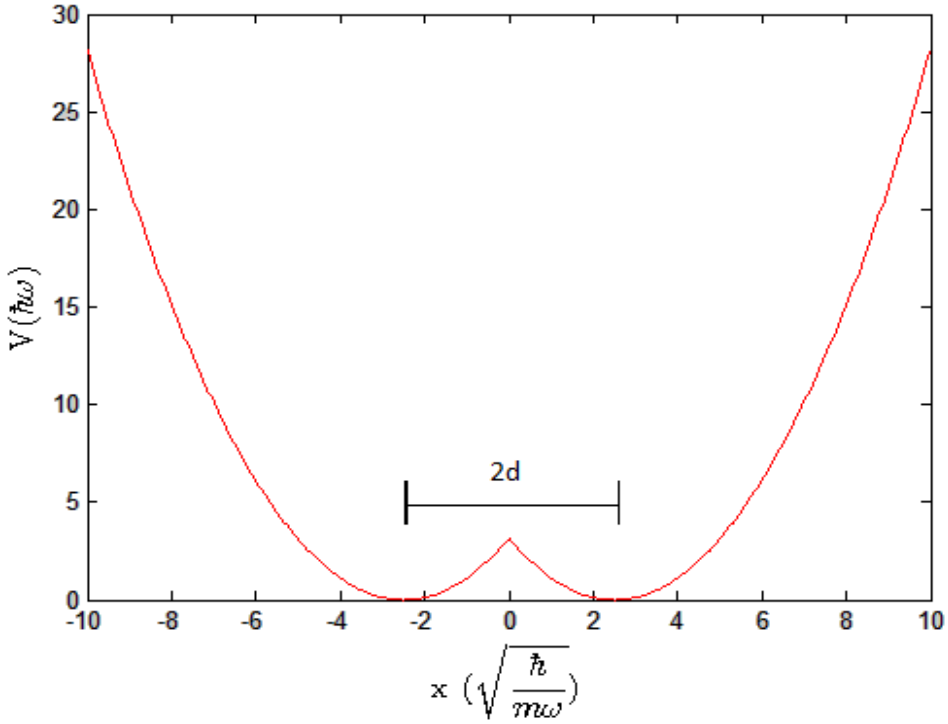

Figure 3.Double-well potential as given by equation (2.5) for $d = 2.5\,L$.

Our objective is to transport the atom from one trap to the other. In order to understand how this can be done, we need to study the eigenfunctions and eigenvalues of the Hamiltonian corresponding to a

single atom in a double-well potential.

In order to analyze the eigenfunctions of such system, let us first consider the case where the separation distance between the two wells is very large. In this case, the two traps can be treated as two separate quantum harmonic oscillators. The eigenfunction for a particular energy eigenvalue of such system can be written as a linear combination of the eigenfunctions of two separate quantum harmonic oscillators that correspond to this energy eigenvalue.

In order to find the coefficients of this linear combination, we should remember that, as mentioned in Section 2.1, any non-degenerate Hamiltonian with a real symmetric potential will have the eigenfunctions that are either odd or even functions. Taking into account this fact and the fact that the wave function has to be normalized, the coefficients of the linear combination must be $\pm\frac{1}{\sqrt{2}}$. Thus, the eigenfunctions of a single neutral atom in a double-well potential in the case of a very large separation distance between the wells can be written as

$$\varphi_{n\pm}=\frac{1}{\sqrt{(2)}}\{\Phi_n(x-d)\pm\Phi_n(x+d)\}, \tag{2.6}$$

where $\Phi_n(u)$ are the eigenfunctions of the quantum harmonic oscillator as in (2.3a). The eigenfunction φ_{n+} corresponds to the symmetric eigenfunctions while φ_{n-} corresponds to the anti-symmetric eigenfunctions.

We are interested in the case where the initial wave function is the ground state of one of the traps. For example we can consider that, initially, the atom is at the right trap, that is $|\Psi(t=0)\rangle=|0\rangle\rightarrow\Psi(x,0)=\Phi_0(x-d)$. Here, we denote the ground state of the right trap as $|0\rangle$ and the ground state of the left trap as $|1\rangle$. The symmetric and anti-symmetric states are denoted as $|+\rangle$ (corresponding to φ_{0+}) and $|\text{-}\rangle$ (corresponding to φ_{0-}), respectively. From equation (2.6), we can write

$$|0\rangle=\frac{1}{\sqrt{(2)}}\{|+\rangle+|\text{-}\rangle\} \tag{2.7a}$$

$$|1\rangle=\frac{1}{\sqrt{(2)}}\{|+\rangle-|\text{-}\rangle\}. \tag{2.7b}$$

Equations (2.7a) and (2.7b) are only valid for a large value of *d*. In order to get the expression of $|+\rangle$ and $|\text{-}\rangle$ for a closer separation distance, let us assume that the ground state of one of the traps is only coupled to the two lowest eigenstates of the double-well potential. That is

$$|0\rangle=a|+\rangle+b|\text{-}\rangle. \tag{2.8a}$$

To get the expression for $|1\rangle$ we use the fact that $\langle x|0\rangle=\Phi_0(x-d)$ and $\langle x|1\rangle=\Phi_0(x+d)$. Since $\Phi_0(x)$ and $\langle x|+\rangle$ are even while $\langle x|\text{-}\rangle$ is an odd function, we can obtain

$$\langle x|1\rangle=\Phi_0(x+d)=\Phi_0(-x-d)=\langle -x|0\rangle$$
$$\langle x|1\rangle=a\langle -x|+\rangle+b\langle -x|\text{-}\rangle=a\langle x|+\rangle-b\langle x|\text{-}\rangle$$
$$|1\rangle=a|+\rangle-b|\text{-}\rangle. \tag{2.8b}$$

From (2.8a) and (2.8b) and by imposing the normalization condition we obtain

$$|+\rangle=\frac{1}{2a}\{|0\rangle+|1\rangle\} \tag{2.9a}$$

$$|\text{-}\rangle=\frac{1}{2b}\{|0\rangle-|1\rangle\}, \tag{2.9b}$$

respectively, where $a=\sqrt{\frac{1+\langle 0|1\rangle}{2}}$ and $b=\sqrt{\frac{1-\langle 0|1\rangle}{2}}$. The comparison between the simulation results and these analytical expressions is shown in Figure 4. Note that only the real part of the wave function is shown. This is because the analytical solution is completely real and the imaginary part obtained in the simulation is negligible. It can be seen that the theoretical results are in agreement with the simulation results for this range of separation distances. A closer look shows that the accuracy of the analytical solution is higher for larger d, as expected.

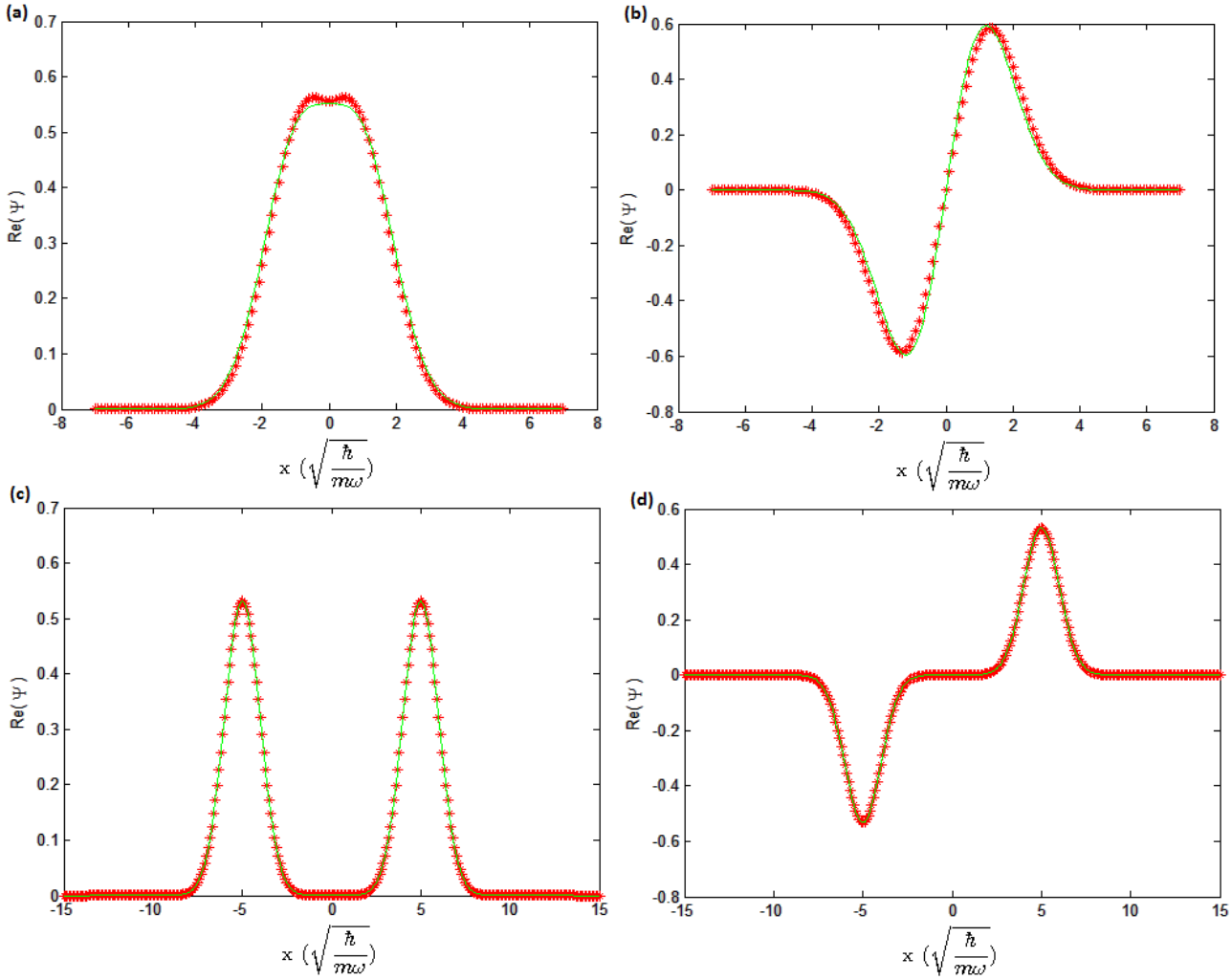

Figure 4. Real part of the eigenfunctions of the symmetric ground state (a,c) and the anti-symmetric ground state (b,d) of a single neutral atom in a double-well potential with $d = L$ (a,b) and with $d = 5L$ (c,d). The red dots (*) are the simulation results while the green lines (——) are the analytical solutions

The eigenvalues corresponding to the symmetric and the anti-symmetric eigenstates can be derived by calculating the energy expectation value for both eigenstates. Of importance to us is the expression of their difference which can be written as

$$\Delta E=\frac{2}{1-\langle 0|1\rangle^2}\{\langle 0|1\rangle\langle 0|\hat{H}|0\rangle-\langle 0|\hat{H}|1\rangle\}, \tag{2.10}$$

where $\hat{H}$ is the Hamiltonian of the system composed by a single neutral atom in a double-well potential.

We can calculate $\langle 0|1\rangle$, $\langle 0|\hat{H}|0\rangle$, and $\langle 0|\hat{H}|1\rangle$ by solving the following integrals.

$$\langle 0|\hat{H}|0\rangle = E_0 + \frac{\hbar\omega}{\sqrt{\pi}}\int_{-\infty}^{0} du\{(\frac{1}{2}(u+\tilde{d})^2 - \frac{1}{2}(u-\tilde{d})^2)e^{-(u-\tilde{d})^2}\}, \tag{2.11a}$$

$$\langle 0|\hat{H}|1\rangle = E_0\langle 0|1\rangle + \frac{\hbar\omega}{\sqrt{\pi}}\int_{0}^{\infty} du\{(\frac{1}{2}(u-\tilde{d})^2 - \frac{1}{2}(u+\tilde{d})^2)e^{-\frac{(u-\tilde{d})^2+(u+\tilde{d})^2}{2}}\}, \tag{2.11b}$$

$$\langle 0|1\rangle = \frac{1}{\sqrt{\pi}}\int_{-\infty}^{\infty} du\{e^{-\frac{(u-\tilde{d})^2+(u+\tilde{d})^2}{2}}\}, \tag{2.11c}$$

where $\tilde{d} = \frac{d}{L}$. The expressions for $\langle 0|\hat{H}|0\rangle$ and $\langle 0|\hat{H}|1\rangle$ are obtained by comparing the Hamiltonian of a single neutral atom in a double-well potential to the Hamiltonian of a single neutral atom in a harmonic potential. The resulted expression for ΔE is

$$\Delta E = \frac{-1+e^{\tilde{d}^2}\{1+\tilde{d}\sqrt{\pi}(1-erf(\tilde{d}))\}}{\sqrt{\pi}(e^{2\tilde{d}^2}-1)/2\tilde{d}}\hbar\omega. \tag{2.12}$$

Let us define the tunneling rate, $\Omega = \frac{\Delta E}{\hbar}$. Figure 5 shows the comparison between the analytical expression of this tunneling rate (i.e. equation (2.12)) and the values obtained from the simulations. As it can be seen, the agreement is very strong.

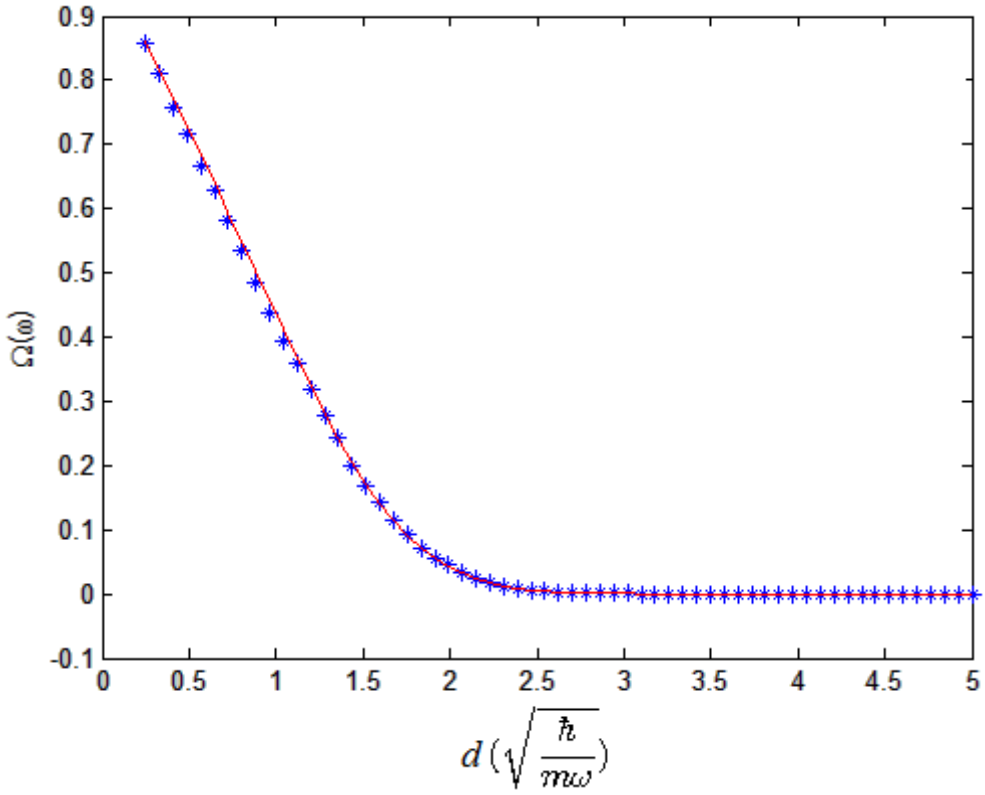

Figure 5. Tunneling rate for the double-well potential as a function of the trap separation, *d*. The blue dots (*) are the simulation results and the red line (——) is the analytical solution given by equation (2.12)

Let us examine how our wave function evolves in time. Using (2.4), (2.9a), (2.9b), and as the initial condition, $|\Psi(t=0)\rangle=|0\rangle$, we obtain, up to an irrelevant space-independent phase,

$$|\Psi(t)\rangle=\cos(\frac{\Omega}{2}t)|0\rangle+i\sin(\frac{\Omega}{2}t)|1\rangle, \tag{2.13}$$

From (2.13), it is clear that the atom oscillates between the right and the left traps.

The contour plot of the numerically obtained spatio-temporal evolution of the probability density for a single atom in a double-well potential with the atom in the ground state of the right trap (i.e. state $|0\rangle$) at the initial time is shown in Figure 6.

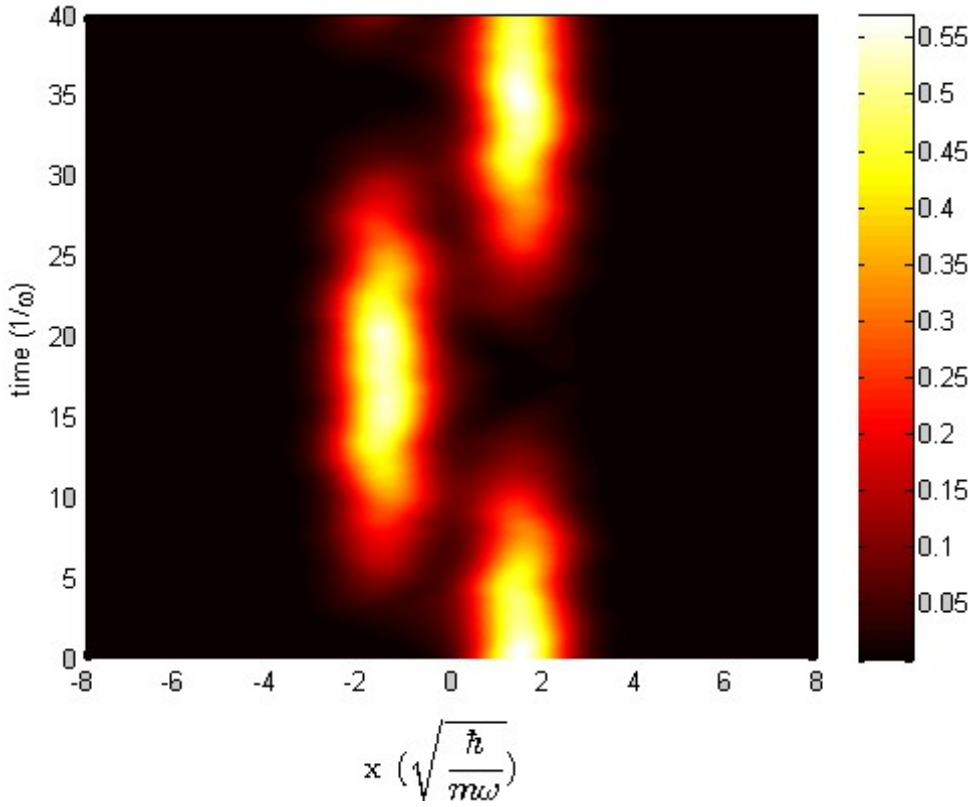

Figure 6. Spatio-temporal evolution of the probability density of a single neutral atom in a double-well potential with d = 1.5L and the initial state being $|0\rangle$, the ground state of the right trap.

Note that there is a strange ripple in Figure 6. This is because equation 2.10(a) is only an approximation. In fact, the state $|0\rangle$ has components that correspond to higher energy eigenstates, not only $|+\rangle$ and $|-\rangle$. We do the same simulation as the one shown in Figure 6 but with a different initial condition. The initial condition is $|\alpha\rangle=a|+\rangle+b|-\rangle$, where a and b are as in equation (2.9(a,b)) and both $|+\rangle$ and $|-\rangle$ are obtained by solving the time-independent Schrödinger equation using the Imaginary Time Propagation method (see Appendix A). The result of this simulation is shown in Figure 7. As it can be seen, in this case, the ripple disappears. This shows that the ripple is, indeed, caused by the coupling to higher energy eigenstates.

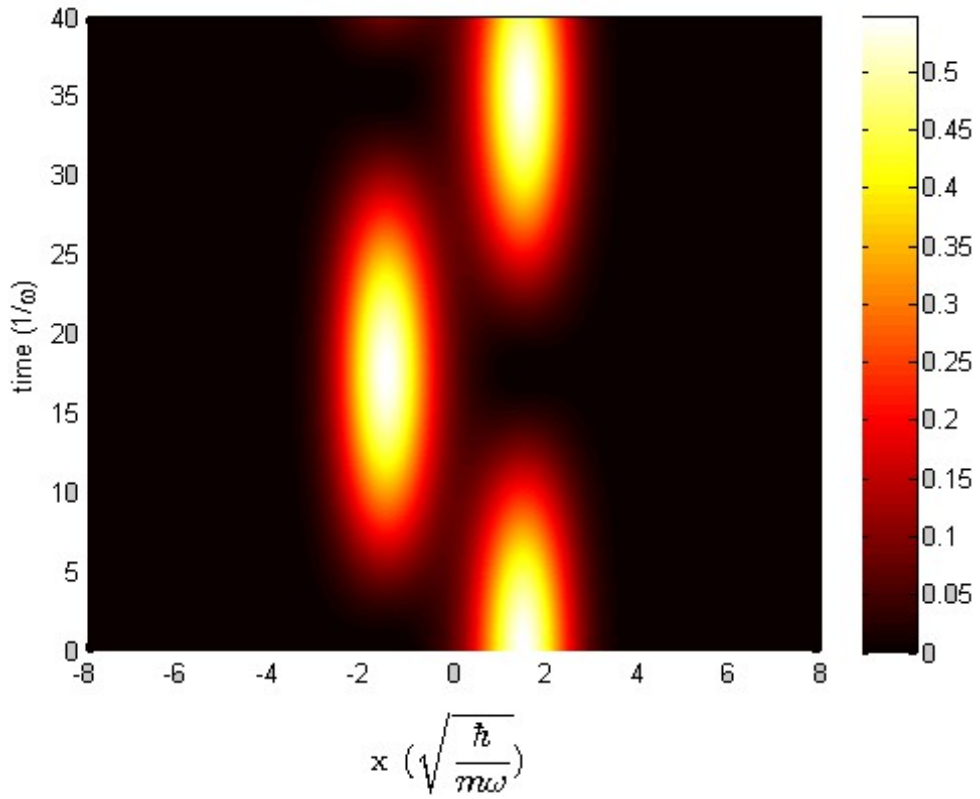

Figure 7. Spatio-temporal evolution of the probability density of a single neutral atom in a double-well potential with d =1.5L and the initial state being $a|+\rangle+b|\text{-}\rangle$ where a and b are as in equation (2.9(a,b)).

Based on Figure 5, the tunneling rate for d =1.5L is $\Omega=0.1776\,\omega$. This is quite close to the simulated tunneling rate observed from Figure 6 and Figure 7 which is equal to $\Omega_{\text{sim}}=0.1789\,\omega$. Hence, we can justify the use of the described analytical model.

The state of a single neutral atom in a double-well potential given in equation (2.13) is similar to the state of an atom modeled as a two internal atomic level system interacting with a resonant electromagnetic field with Rabi frequency, $\Omega_{rabi}=\frac{\mu\,\varepsilon}{\hbar}$. Here, μ is the transition electric dipole moment along the electric field direction and ε is the amplitude of the electric field. It is known that, if this system is initially in one eigenstate of the bare system, applying a time-varied Rabi frequency such that the pulse area defined by $\int_0^t \mathrm{d}\,t'\,\Omega_{rabi}(t')$ has a value equal to π , the atom will be transferred to the other eigenstate at time t.

Using the analogy between the tunneling and the Rabi oscillation, a procedure to perform a coherent transport of an atom between two traps is derived in [3]. In the method explained there, the tunneling rate is manipulated by moving one of the traps such that the pulse area, $\int_0^t \mathrm{d}\,t'\,\Omega(t')=\pi$ where $\Omega(t')$ is the time-varied tunneling rate. It is also possible to move both of the traps as long as the pulse area condition is satisfied.

We take that the initial and the final distance between the two traps is equal to the maximum distance. The time needed for the tunneling-based transport depends on this maximum and minimum allowed distance between the two traps. Generally speaking, the time will be shorter if

these two parameters are smaller. There are two reasons for this. The first one is quite obvious: smaller distances between the two traps result in larger tunneling rates. Hence, shorter time is needed to achieve the required pulse area. The second reason is related to the adiabatic transport of an atom. As stated in [3], in order to not populate the excited states, the trap has to be moved adiabatically. This means that the couplings between the current eigenstate and other energy eigenstates have to be much lower than their energy differences. Mathematically, it can be written as [15]:

$$\left|\langle m;t|\frac{\partial}{\partial t}|n;t\rangle\right| \ll \frac{E_m}{\hbar}, \tag{2.14}$$

where $|m\rangle$ is the current eigenstate, $|n\rangle$ is any eigenstate other than $|m\rangle$, and the index t indicates that the eigenstates are time dependent. Given the trajectory of the trap, it is possible to relate the maximum allowed speed of the trap and the maximum distance to be reached (for an example of this calculation, see Appendix B). However, since we deal with two traps and not one single isolated trap, the exact calculation is not straightforward. Regardless, it is still true that there is an upper limit for the speed of the moving trap if we want to fulfill (2.14).

In our simulation, initially the atom is in the right trap. The left trap then moves with velocity

$$v(t) = \begin{cases} \frac{\pi x_{max}}{2T_{app}}\sin\left(\frac{\pi t}{T_{app}}\right), & 0 \le t \le T_{app} \\ 0, & T_{app} < t \le T_{app} + T_{\text{int}} \\ \frac{-\pi x_{max}}{2T_{app}}\sin\left(\frac{\pi t}{T_{app}}\right), & T_{app} + T_{\text{int}} < t \le 2T_{app} + T_{\text{int}} \\ 0, & t > 2T_{app} + T_{\text{int}} \end{cases}$$

where T_{app} is the total approaching (separating) time, T_{int} is the total time the left trap spends at the minimum distance from the right trap, and x_{max} is the the difference between the maximum distance and the minimum distance between the two traps. The total processing time can be calculated as $T = 2T_{app} + T_{\text{int}}$.

In our simulation, we use $x_{max} = 14.4L$ and the minimum separation distance is equal to $3.6L$. The value of $T_{app} = \frac{144}{\omega}$ is used. To ensure that the pulse area is equal to π, the value of $T_{\text{int}} = \frac{23.184}{\omega}$ is used . Hence, the total processing time is $T = \frac{167.184}{\omega}$. Based on the results of our simulation, the population of the excited states can be neglected in this case.

The contour plot of the spatio-temporal evolution of the potential and that of the probability density are shown in Figure 8(a) and 8(b), respectively. The plots of the time evolution of the distance between the traps and of the tunneling rate are shown in Figure 8(c) and 8(d), respectively. For completeness, the plot of the time evolution of the population in each trap is shown in Figure 8(e) and the snapshots of the potential and of the probability density at three different times during the process are shown in Figure 8(f).

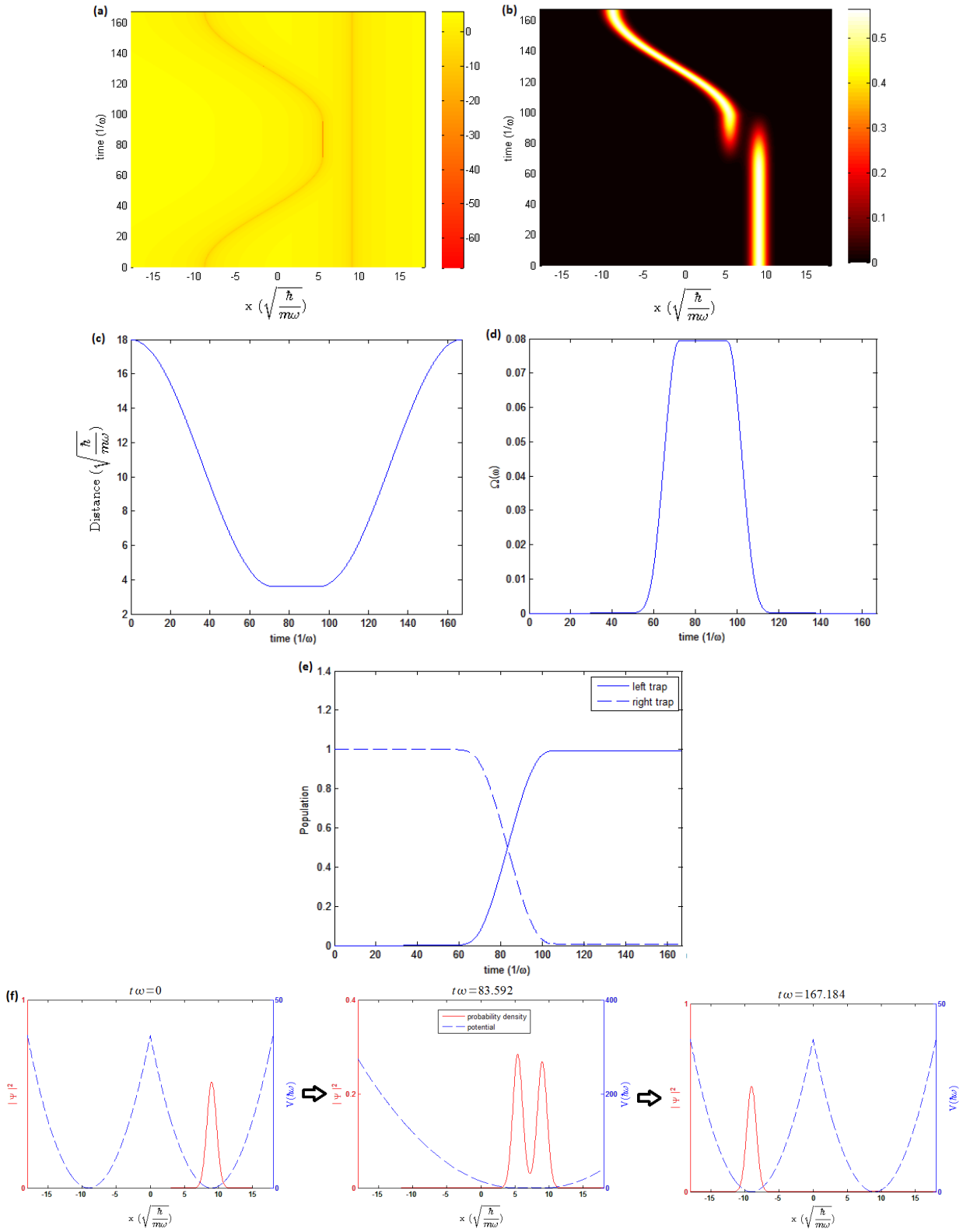

Figure 8. Simulation of the coherent population transfer of a single neutral atom between two traps using tunneling. Here we show the spatio-temporal evolution of $\ln\left(V\left(x,t\right)\right)$ (in units of $\hbar\omega$) (a) and of the probability density (b), the time evolution of the distance (c) and of the tunneling rate between the traps (d), the time evolution of the population in each trap (e), and the snapshots of the potential and the probability density at three different times (f). We use $x_{max}=14.4\,L$, the minimum separation distance $3.6L$, $T=\frac{167.184}{\omega}$, and $T_{\text{int}}=\frac{23.184}{\omega}$.

The population in each trap, in the case of the double-well potential, is defined as

$$P_{\text{right}}(t)=\int_{x_{mid}(t)}^{x_{upper}} \mathrm{d}x\,|\Psi(x,t)|^2,$$
$$P_{\text{left}}(t)=\int_{x_{lower}}^{x_{mid}(t)} \mathrm{d}x\,|\Psi(x,t)|^2, \tag{2.15}$$

where $x_{mid}(t)$ is the middle point between the traps while x_{upper} and x_{lower} are the upper and lower boundaries of the simulation space, respectively. We define the transfer efficiency as $\eta=\frac{P_{ff}}{P_{ii}}$ where P_{ff} is the population in the destination trap at the end of the process and P_{ii} is the population in the initial trap at the initial time. In our simulation, $\eta=99.25\%$ is obtained.

2.3. Three-Level Atom Optics

As it has been discussed in Section 2.2, a system of a single neutral atom in a double-well potential can be modeled as a system consisting of two internal atomic levels interacting with a resonant electromagnetic field. The basic idea of the Three-Level Atom Optics (TLAO) [4] concept is to extend this analogy to a system of a single neutral atom in a triple-well potential. The considered triple-well potential is illustrated in Figure 9 for $d_1 = d_2 = 9L$. In general, d_1 can be different than d_2.

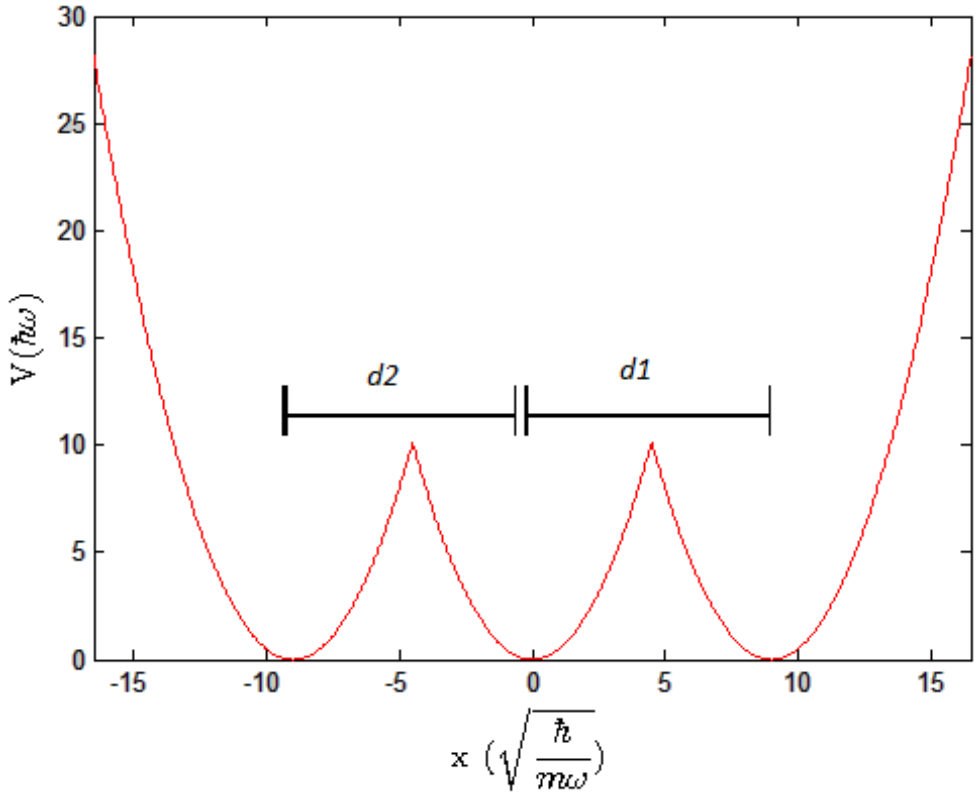

Figure 9. Triple-well potential. The values $d_1 = d_2 = 9L$ are used.

Assuming that the couplings happen only between the right trap and the middle trap and between the left trap and the middle trap, a system of a single atom in a triple-well potential can be modeled as a three internal atomic level system interacting with two resonant electromagnetic fields (see Figure 10). In this figure, $\Omega_i, i=1,2$ represent the corresponding Rabi frequencies of the fields.

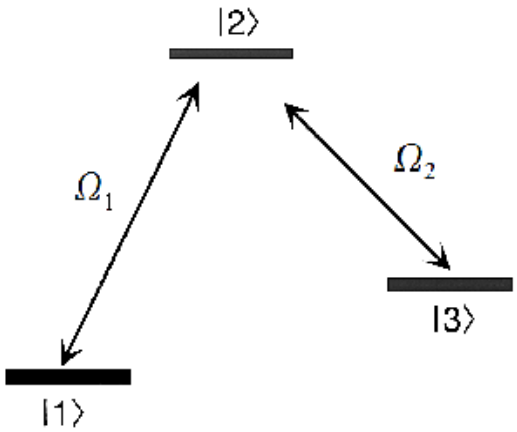

Figure 10. Three-level system interacting with two electromagnetic fields with Rabi frequencies Ω_1 and Ω_2, respectively.

The Hamiltonian of such system in the interaction picture under the Rotating Wave Approximation (RWA) and the Electric Dipole Approximation (EDA) can be expressed as [16]:

$$H = \frac{\hbar}{2}\begin{bmatrix} 0 & \Omega_1(t) & 0 \\ \Omega_1(t) & 0 & \Omega_2(t) \\ 0 & \Omega_2(t) & 0 \end{bmatrix},$$

where columns 1, 2, 3 correspond to states $|1\rangle, |2\rangle, |3\rangle$, respectively. The eigenvalues of such Hamiltonian are

$$\hbar\omega^- = -\hbar\sqrt{\Omega_1^2+\Omega_2^2}, \tag{2.16a}$$

$$\omega^0 = 0 \tag{2.16b}$$

$$\hbar\omega^+ = \hbar\sqrt{\Omega_1^2+\Omega_2^2}, \tag{2.16c}$$

The eigenstate corresponding to ω^0 is called the dark state and can be expressed as

$$|a^0\rangle = \cos(\Theta)|1\rangle - \sin(\Theta)|3\rangle, \tag{2.17}$$

where the mixing angle Θ is defined as $\tan(\Theta) = \frac{\Omega_1}{\Omega_2}$. Thus, starting with the atom in $|1\rangle$ and changing this mixing angle from 0 to $\frac{\pi}{2}$ by following the dark state adiabatically, we can transfer the population from $|1\rangle$ to $|3\rangle$ efficiently. This is the basic idea of the Stimulated Raman Adiabatic Passage (STIRAP) technique [16]. This technique allows a robust population transfer between two energy levels of an atom or a molecule. The adiabaticity condition can be written as [16]:

$$\left|\frac{d\Theta}{dt}\right| \ll \left|\omega^{\pm}(t) - \omega^0\right| = \sqrt{\Omega_1^2(t)+\Omega_2^2(t)}. \tag{2.18}$$

When the two pulses have the same shape, the adiabaticity condition can be simplified to [16]:

$$\Omega_{eff}\Delta\tau > k, \tag{2.19}$$

where $\Delta\tau$ is the duration of a period during which the two pulses have significant overlap and $\Omega_{eff} = \sqrt{\Omega_1^2+\Omega_2^2}$ is the rms Rabi frequency. The value of parameter *k* is around 10 for optimum shape and pulse delay [16].

Following the same reasoning as in STIRAP, a similar technique can be implemented for the transport of a single neutral atom between the two extreme traps of a triple-well potential. The

technique is described in [4] and it is called Three-Level Atom Optics (TLAO).

Let us analyze the following scenario: the atom is in the right trap at the initial time and it should be transferred to the left trap at the final time. Using the analogy with the three internal atomic level system, the ground state of the right trap, the middle trap, and the left trap play the role of $|1\rangle$, $|2\rangle$ and $|3\rangle$, respectively. The tunneling rate between the middle trap and the right trap is analogous to Rabi frequency between $|1\rangle$ and $|2\rangle$ while the tunneling rate between the middle trap and the left trap is analogous to Rabi frequency between $|3\rangle$ and $|2\rangle$. Changing the tunneling rate is accomplished by moving the left trap or the right trap to be closer to or further from the middle trap. The sequence of movement should be such that the mixing angle changes from 0 to $\frac{\pi}{2}$ by adiabatically following the dark state given in (2.17). This can be done if the left trap approaches and separates from the middle trap and, with a certain time delay, the right trap approaches and separates from the middle trap.

The adiabaticity condition is given by equation (2.19). Since the left hand side is proportional to the pulse area, we can also write the adiabaticity condition in term of the pulse area, $\int_0^T \mathrm{d}t'\,\Omega(t')$ where T is the total processing time and $\Omega(t')$ is the time-varied tunneling rate. The minimum requirement for the pulse area can be obtained numerically.

The population in each trap is defined as

$$\begin{aligned} P_{\text{right}}(t) &= \int_{x_{mid1}(t)}^{x_{upper}} \mathrm{d}x\,|\Psi(x,t)|^2, \\ P_{\text{middle}}(t) &= \int_{x_{mid2}(t)}^{x_{mid1}(t)} \mathrm{d}x\,|\Psi(x,t)|^2, \\ P_{\text{left}}(t) &= \int_{x_{lower}}^{x_{mid2}(t)} \mathrm{d}x\,|\Psi(x,t)|^2, \end{aligned} \tag{2.20}$$

where $x_{mid1}(t)$ and $x_{mid2}(t)$ are the middle points between the right trap and the middle trap and that between the left trap and the middle trap, respectively, while x_{upper} and x_{lower} are the upper and lower boundaries of the simulation space, respectively.

In our simulation, initially the atom is in the right trap. The initial distance between the left trap and the middle trap is the same as the initial distance between the right trap and the middle trap. The left trap then moves with velocity

$$v_L(t) = \begin{cases} \frac{\pi x_{max}}{T_1}\sin\left(\frac{2\pi t}{T_1}\right), & 0 \le t \le T_1 \\ 0, & t > T_1 \end{cases} \tag{2.21a}$$

while the right trap moves with velocity

$$v_R(t) = \begin{cases} 0, & t < T_d \\ \frac{-\pi x_{max}}{T_1}\sin\left(\frac{2\pi(t-T_d)}{T_1}\right), & T_d \le t < T_d + T_1 \\ 0, & t > T_d + T_1 \end{cases} \tag{2.21b}$$

where T_1 is the total approaching and separation time, T_d is the time delay between the moment at which the left trap starts to move and the moment when the right trap starts to move, and x_{max} is the difference between the maximum and the minimum distance between the left (right) trap and the middle trap. The total processing time can be calculated as $T = T_1 + T_d$.

The results of our simulation are shown in Figure 11. The final and initial distances used are the same as in the case for the tunneling-based transport discussed in Section 2.2. We find that $T_d : T_1 = 4:21$ gives optimum transfer efficiency. Using the optimum pulse delay, a pulse area bigger than 19 is needed to obtain transfer efficiency bigger than 99.5%. This corresponds to a requirement of processing time bigger than $\frac{162}{\omega}$. In our simulation, we use $T = \frac{165}{\omega}$ as the total time of the transport process with the pulse delay equal to $T_d = \frac{26.4}{\omega}$.

The contour plot of the spatio-temporal evolution of the potential (in logarithmic scale) and of the probability density are shown in Figure 11(a) and 11(b), respectively. The plots of the time evolution of the distances between the traps and that of the tunneling rates are shown in Figure 11(c) and 11(d), respectively. For completeness, the plot of the time evolution of the population in each trap is shown in Figure 11(e) and the snapshots of the potential and the probability density at three different times during the transport process are shown in Figure 11(f). In our simulation, we achieved $\eta = 99.57\%$ for this TLAO-based transport. Note also that the population in the middle trap is not zero because the procedure is done in finite time. If we increase the processing time, the population in the middle trap will decrease.

From the simulation results, we can see that the transfer efficiency of the TLAO-based transport is better than the tunneling-based transport for equal processing time. This is true if the adiabaticity condition for the TLAO-based transport is fulfilled. If the adiabaticity condition is not fulfilled then the tunneling-based transport has higher transfer efficiency than the TLAO-based transport. For example, with the processing time equal to $\frac{110}{\omega}$, the adiabaticity condition for the TLAO-based transport is not fulfilled. For this processing time, we find that $\eta = 99\%$ for the tunneling-based transport and $\eta = 88.46\%$ for the TLAO-based transport. Hence, in general, we can say that the TLAO-based transport is slower than the tunneling-based transport.

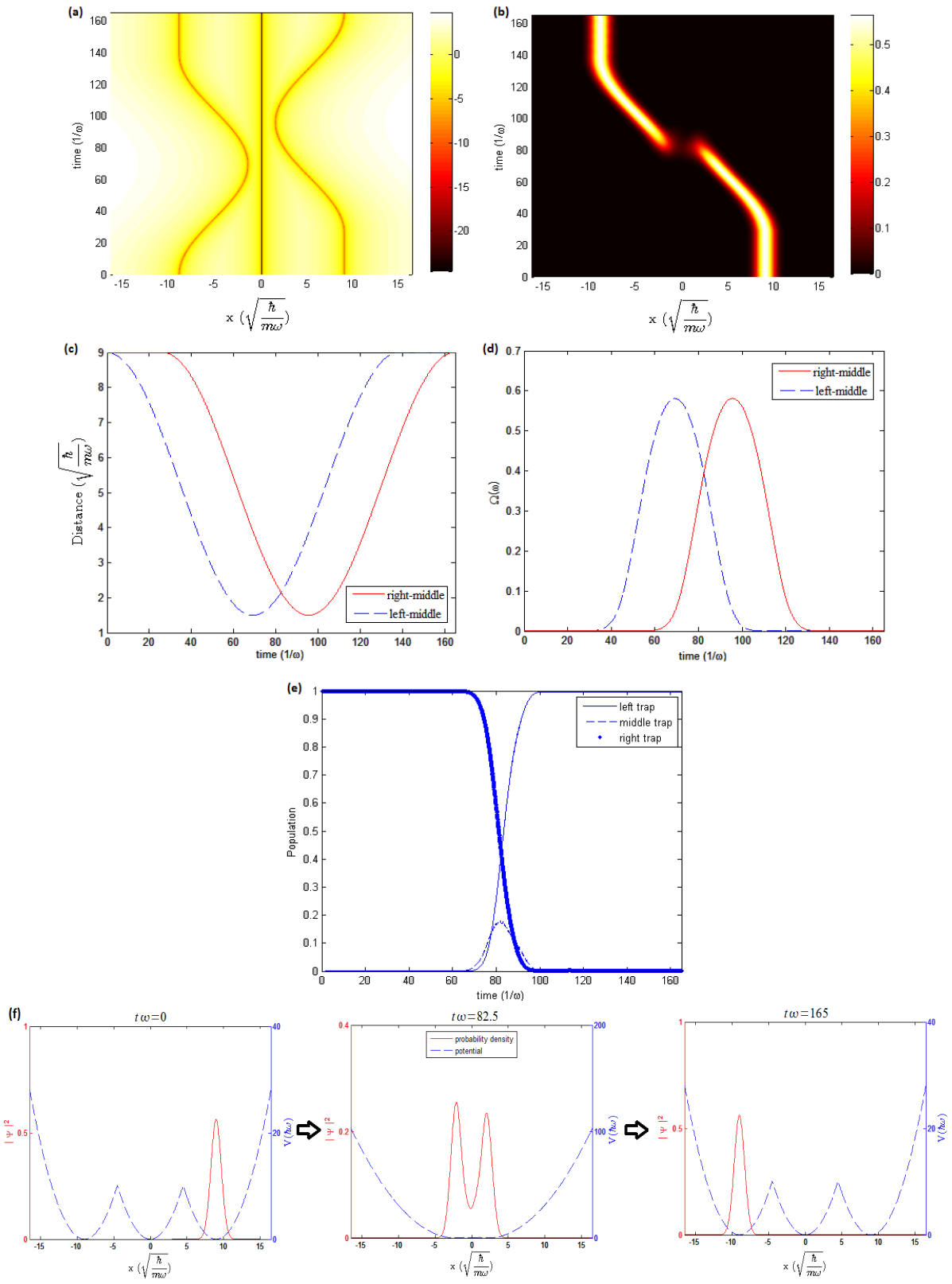

Figure 11. Simulation of the coherent population transfer of a single neutral atom between two traps using TLAO-based transport. Here we show the spatio-temporal evolution of $\ln(V(x,t))$ (in units of $\hbar\omega$) (a) and of the probability density (b), the time evolution of the distances (c) and of the tunneling rates between the traps (d), the time evolution of the population in each trap (e), and the snapshots of the potential and the probability density at three different times (f). The total time $T=\frac{165}{\omega}$ with the pulse delay $T_d=\frac{26.4}{\omega}$ are used.

The main advantage of the TLAO-based transport is its robustness against experimental imperfections [4]. For the tunneling-based transport, the change in the pulse area can be significant for a small change in the interaction time. Since the transfer efficiency of the tunneling-based transport is highly dependent on the pulse area, this technique is very sensitive to the variation in the interaction time. This is not the case for TLAO-based transport if the adiabaticity condition (2.19) is fulfilled since it follows an eigenstate of the system [4].

We study the effect of the shaking and tilting of the experimental setup as well as the effect of limited spatial and temporal resolution of the potential to the transfer efficiency of the tunneling-based transport and the transfer efficiency of the TLAO-based transport. The shaking is simulated by introducing a time-dependent horizontal displacement, $\Delta x(t) = A_s \sin(\omega_s t)$ to the potential. For simulating the tilting of the experimental setup, we add a tilted potential, $V_{tilt} = \beta \hbar \omega \frac{x}{L}$ to the original potential. The effect of limited spatial and temporal resolution of the potential is studied by applying a low pass filter to the potential in space and time, respectively. The spatial resolution is expressed in terms of the pixel pitch while the temporal resolution is given in terms of the refresh period of the potential. The results are shown in Figure 12.

From Figure 12(a) and (b), we can see that for a wide range of shaking amplitudes and frequencies, both methods are robust. Also, the TLAO-based transport is more robust for high shaking amplitude. As can be seen from Figure 12(c), the TLAO-based transport is also more robust against the tilting of the experimental setup. Regarding the limited spatial and temporal resolution, we can see from Figure 12(d) and (e) that, in general, the TLAO-based transport has higher transfer efficiency compared to the tunneling-based transport for the same spatial and temporal resolution of the potential. Thus, it is expected that the TLAO-based transport will be more robust than the tunneling-based transport in a real experimental setting.

One possible way to implement the TLAO-based transport is by using a spatial light modulator (SLM). The use of SLM in creating spatio-temporal dependent potential for Bose-Einstein condensate [17] and cold atoms [18] has been reported. SLM has also been used in experiments related to transport of an atom and in quantum information processing [19, 20].

We can make a rough estimate to the requirement of the SLM needed to realize the TLAO based transport. As it can be seen from Figure 12(d) and (e), to obtain $\eta \geq 90\%$ for the TLAO-based transport, we need a pixel pitch smaller than $2L$ and a refresh rate larger than $\frac{\omega}{13}$. As stated in [3], for ^{87}Rb atom, the typical trapping frequency, ω, are 10^5 to 10^6 Hz. Using the value of $\omega = 10^5$ Hz, we can obtain L = 85 nm for ^{87}Rb atom. Hence, we will need a SLM with pixel pitch smaller than 170 nm and and refresh rate larger than 7.7 kHz. The state-of-the-art SLM can not fulfill this requirement. For example, a Linear series of Boulder Nonlinear System SLM only has a pixel pitch of $1.6 \mu m$ with a maximum refresh rate 200 Hz [21]. A higher refresh rate up to 1 kHz can be achieved for different kind of SLM [22].

It is possible to combine the use of SLM with other optical devices to overcome this limitation. For example, we can demagnify the image produced by the SLM to obtain a higher spatial resolution of the potential [17]. Another approach is to combine the SLM with the Acousto-Optic-Modulator (AOM) to improve both the temporal and spatial resolution of the potential [18].

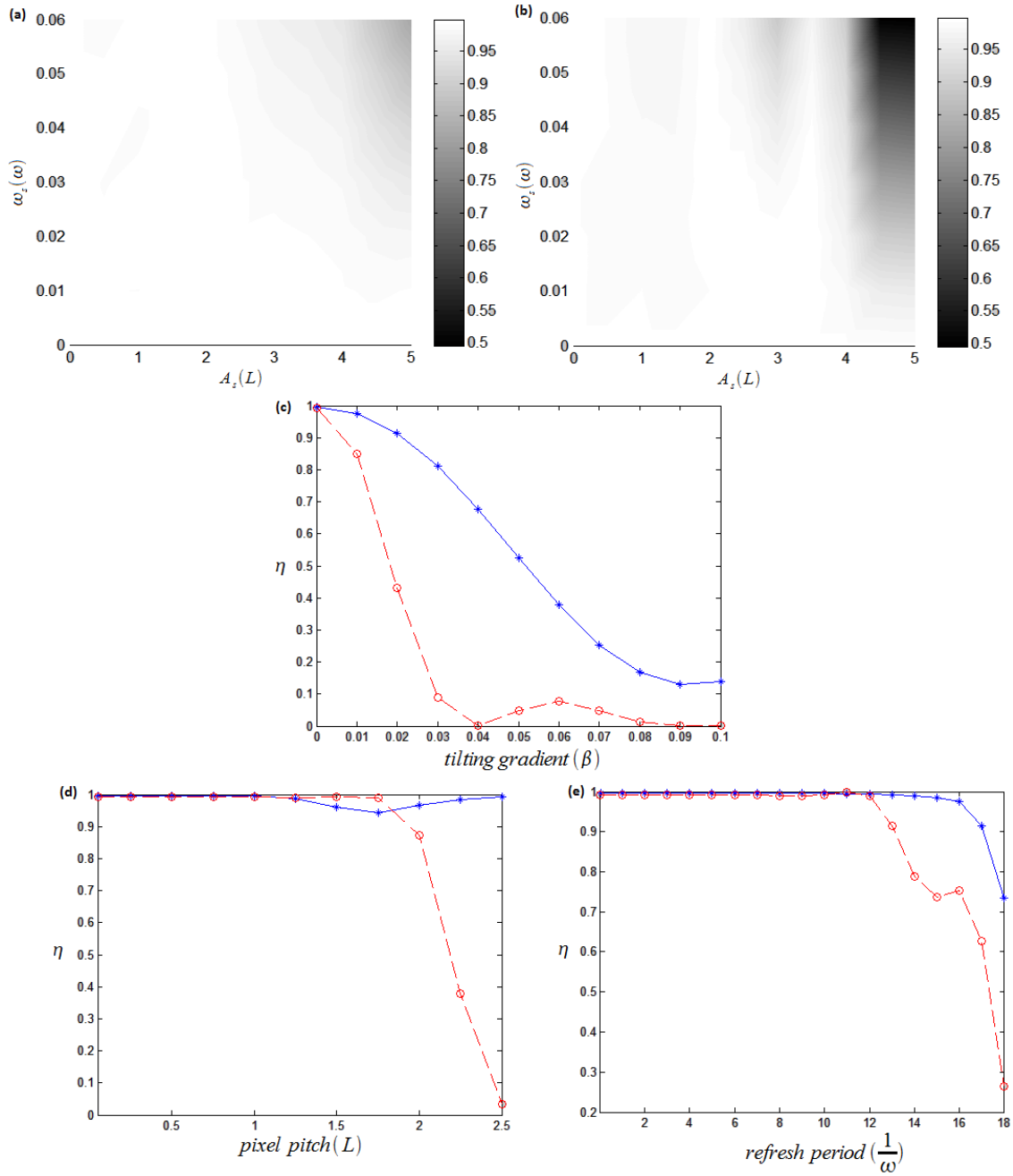

Figure 12. Comparison between the robustness of the TLAO-based transport and the tunneling-based transport. Transfer efficiency of the TLAO-based transport (a) and of the tunneling-based transport (b) as a function of the shaking amplitude (A_s) and the shaking frequency (ω_s) are shown. In (c), (d), and (e) the blue line with star marks (—✳—) and the red dashed line with dot marks (—○—) represent the results for the case of the TLAO-based transport and the tunneling-based transport, respectively. Transfer efficiency as a function of the tilting gradient, β , is shown in (c). The effect of limited spatial and temporal resolution of the SLM is shown in (d) and (e), respectively.

Up to the author's knowledge, at the time this report is written, there has not been any experiment conducted to realize the TLAO-based transport of a single neutral atom. Nevertheless, it is worth mentioning that the experimental demonstration of spatial adiabatic passage for light has been reported [23,24].

As a conclusion, in this chapter, we have reviewed the quantum dynamics of a single neutral atom in single, double-well, and triple-well harmonic potentials. Two transport procedures are reviewed. They are the tunneling-based transport and the TLAO-based transport. The TLAO-based transport has the advantage of higher robustness against experimental imperfections while the tunneling-based transport has the advantage of a lower processing time. In the next chapter, we will discuss how we can accelerate the quantum dynamics of the TLAO-based transport.

CHAPTER THREE

Fast-Forward technique for the transport of a neutral atom

As stated in the previous chapter, one of the main drawbacks of the Three-Level Atom Optics (TLAO) based transport of a single neutral atom is the long processing time needed due to the adiabaticity condition.

In this chapter we will explain how this problem can be solved using the Fast-Forward technique [11]. Our objective is to design a potential, *V(x,t)*, such that the wave function, $\Psi(x,t)$, acquires the desired form in a shorter time compared to the time needed by the usual TLAO-based transport.

We start this chapter by describing the Fast-Forward technique [11]. We then describe the extension of this Fast-Forward technique to the case where the initial process is adiabatic. In this later case, the aim is to obtain a shortcut to adiabaticity that is based on the Fast-Forward technique [10]. We then discuss a simple example of the fast-forwarding of the adiabatic translation of a single atom. The main result regarding the fast-forwarding of the TLAO-based technique is given at the end of this chapter.

3.1. Fast-Forward technique and shortcut to adiabaticity

The 1D fast-forward problem in quantum mechanics (see [11]) can be stated as follow:

Given a potential $V_0(x,t)$ and the solution of the Schrödinger equation,

$$i\hbar\frac{\partial}{\partial t}\Psi_0(x,t)=\left(\frac{-\hbar^2}{2m}\frac{\partial^2}{\partial x^2}+V_0(x,t)\right)\Psi_0(x,t),$$

find a new potential $V_{FF}(x,t)$ such that the solution of the Schrödinger equation,

$$i\hbar\frac{\partial}{\partial t}\Psi_{FF}(x,t)=\left(\frac{-\hbar^2}{2m}\frac{\partial^2}{\partial x^2}+V_{FF}(x,t)\right)\Psi_{FF}(x,t),$$

is the fast-forwarded state $\Psi_{FF}(x,t)=\Psi_0(x,\Lambda(t))$ where $\Lambda(t)=\int_0^t \mathrm{d}t'\alpha(t')$ with $\alpha(t)\geq 1$ and $\Lambda(t)>t, \forall t>0$.

The parameter $\alpha(t)$ is called the magnification factor. The requirement is that $\alpha(t)=1$ and $\frac{d\alpha}{dt}=0$ at the initial and final time. In the intermediate time, we require $\alpha(t)\geq 1$ because we are interested in speeding up the quantum dynamics. The case where $\alpha(t)\leq 1$ and $\Lambda(t)<t, \forall t>0$ corresponds to the slowing down of the quantum dynamics.

One can prove that fast-forwarding is impossible by using the continuity equation. The continuity equation for a wave function $\Psi(x,t)$ can be written as

$$-\frac{\partial}{\partial t}(\Psi^*\Psi)=\frac{\hbar}{m}\frac{\partial}{\partial x}\{\Im\{\Psi^*\frac{\partial\Psi}{\partial x}\}\} \ .$$

Applying the continuity equation to $\Psi_{FF}(x,t)=R(x,\Lambda(t))e^{i\theta(x,\Lambda(t))}$ and $\Psi_0(x,t)=R(x,t)e^{i\theta(x,t)}$, we obtain:

$$-\frac{\partial}{\partial t}R^2(x,\Lambda(t))=\frac{\hbar}{m}\frac{\partial}{\partial x}\{R^2(x,\Lambda(t))\frac{\partial\theta(x,\Lambda(t))}{\partial x}\}$$
$$-\alpha(t)\frac{\partial}{\partial t'}R^2(x,t')|_{t'=\Lambda(t)}=\frac{\hbar}{m}\frac{\partial}{\partial x}\{R^2(x,t)\frac{\partial\theta(x,t')}{\partial x}\}|_{t'=\Lambda(t)}\ , \tag{3.1a}$$

and

$$-\frac{\partial}{\partial t}R^2(x,t)=\frac{\hbar}{m}\frac{\partial}{\partial x}\{R^2(x,t)\frac{\partial\theta(x,t)}{\partial x}\}\ . \tag{3.1b}$$

Comparing (3.1a) and (3.1b), one can see that both expressions can only be fulfilled if $\alpha(t)=1,\forall t$. This means that it is not possible to do the fast-forwarding.

However, if we relax the requirement to $|(\Psi_{FF}(x,t))|=|(\Psi_0(x,\Lambda(t)))|=R(x,\Lambda(t))$, the fast-forwarding of the process can be done. This is the main idea of the Fast-Forward technique.

Here we will derive the fast-forward potential, $V_{FF}(x,t)$, following a different route than the one presented in [11]. We start with the continuity equation to get the requirement for the phase of the fast-forwarded state. Then, we use the Hamilton-Jacobi equation to find the expression of $V_{FF}(x,t)$ in terms of the phase and the amplitude of $\Psi_0(x,\Lambda(t))$ and the original potential $V_0(x,t)$. Our discussion here is valid for the case where relativistic effects can be neglected.

3.1.1. Derivation of the fast-forward potential

Let us write $\Psi_0(x,t)=R(x,t)e^{i\theta(x,t)}$ and $\Psi_{FF}(x,t)=R(x,\Lambda(t))e^{i\theta_{FF}(x,t)}$. Applying the continuity equation to $\Psi_{FF}(x,t)$ we obtain

$$-\alpha(t)\frac{\partial}{\partial t'}R^2(x,t')|_{t'=\Lambda(t)}=\frac{\hbar}{m}\frac{\partial}{\partial x}\{R^2(x,\Lambda(t))\frac{\partial\theta_{FF}(x,t)}{\partial x}\}\ . \tag{3.2}$$

By inserting (3.1b) into (3.2), we obtain

$$\frac{\partial\theta_{FF}(x,t)}{\partial x}=\alpha(t)\frac{\partial\theta(x,\Lambda(t))}{\partial x}$$
$$\theta_{FF}(x,t)=\alpha(t)\theta(x,\Lambda(t))+h(t), \tag{3.3}$$

where $h(t)$ is an arbitrary function of time. We will just use $h(t) = 0$. Note also that, by imposing this and by imposing that $\alpha(t)=1$ at the initial time and the final time, we obtain $\theta_{FF}(x,t)=\theta(x,\Lambda(t))$ at the initial time and the final time.

The Hamilton-Jacobi equation for $\Psi_0(x,t)$ is

$$V_0(x,t)=\frac{\hbar^2}{2m}\frac{1}{R(x,t)}\frac{\partial^2R(x,t)}{\partial x^2}-\frac{\hbar^2}{2m}(\frac{\partial\theta(x,t)}{\partial x})^2-\hbar\frac{\partial\theta(x,t)}{\partial t}\ . \tag{3.4}$$

Using equations (3.3) and (3.4) in the Hamilton-Jacobi equation for $\Psi_{FF}(x,t)$, we can get the expression for $V_{FF}(x,t)$.

$$V_{FF}(x,t)=V_0(x,\Lambda(t))-\hbar\theta(x,\Lambda(t))\frac{\partial\alpha}{\partial t}$$
$$-(\alpha^2(t)-1)\{\hbar\frac{\partial\theta(x,t')}{\partial t'}|_{t'=\Lambda(t)}+\frac{\hbar^2}{2m}(\frac{\partial\theta(x,\Lambda(t))}{\partial x})^2\}. \tag{3.5}$$

This expression is different from the one derived in [11]. However, it can be proved that both are equivalent. The proof can be found in Appendix C.

We can also get another expression of $V_{FF}(x,t)$ by using (3.4) to replace

$\{\hbar\frac{\partial\theta(x,t')}{\partial t'}|_{t'=\Lambda(t)}+\frac{\hbar^2}{2m}(\frac{\partial\theta(x,\Lambda(t))}{\partial x})^2\}$ in (3.5). In this case, we obtain

$$V_{FF}(x,t)=V_0(x,\Lambda(t))-\hbar\theta(x,\Lambda(t))\frac{\partial\alpha}{\partial t} \\ -(\alpha^2(t)-1)\{\frac{\hbar^2}{2m}\frac{1}{R(x,\Lambda(t))}\frac{\partial^2 R(x,\Lambda(t))}{\partial x^2}-V_0(x,\Lambda(t))\}. \quad (3.6)$$

Note that, since we impose $\alpha(t)=1$ and $\frac{d\alpha}{dt}=0$ at the initial time and the final time, we obtain $V_{FF}(x,t)=V_0(x,\Lambda(t))$ at the initial time and the final time regardless which expression of $V_{FF}(x,t)$ we use.

The derivation of the Fast-Forward technique above hints that there is a relation between the Fast-Forward technique and Bohmian mechanics [25]. In Bohmian mechanics, the dynamics of the Schrödinger equation is unraveled in terms of trajectories guided by a pilot wave [26]. In the language of Bohmian mechanics, the Fast-Forward technique consists of the following steps:

*) Multiply the trajectory velocity, $v_T=\frac{\hbar}{m}\frac{\partial\theta(x,\Lambda(t))}{\partial x}$ by the magnification factor $\alpha(t)$ to get the new trajectory velocity.
*) Find the quantum potential that corresponds to the new trajectory velocity.

3.1.2. Implementation of the Fast-Forward technique

In the implementation of this Fast-Forward technique, the main difficulties occur when $R(x,\Lambda(t))\to 0$. Since the simulation program has to divide the imaginary part of the wave function with its real part to get the phase of the wave function, we will encounter an indeterminacy as $R(x,\Lambda(t))\to 0$. This means that the values of $\theta(x,t)$ at the positions where $R(x,\Lambda(t))\to 0$ which are obtained from the simulation can not be trusted. This problem also exists for the other forms of $V_{FF}(x,t)$ (i.e. equations (3.6) and (C.5) in Appendix C).

In order to solve this problem, let us first discuss the following scenario. Instead of applying $V_{FF}(x,t)$ that is calculated using the Fast-Forward formulation, we apply a different potential, $V^a_{FF}(x,t)$. We would like to study how the difference between the resulted wave function, $\Psi^a_{FF}(x,t)$, and the targeted fast-forwarded wave function, $\Psi_{FF}(x,t)=R(x,\Lambda(t))e^{i\theta_{FF}(x,t)}$, is related to the difference between $V^a_{FF}(x,t)$ and $V_{FF}(x,t)$.

Let us write $V^a_{FF}(x,t)=V_{FF}(x,t)+\Delta V(x,t)$. Assume that $\Psi^a_{FF}(x,t_0)=\Psi_{FF}(x,t_0)$ at some $t=t_0$. For $t=t_0+\Delta t$, with $\Delta t\to 0$, we can obtain

$$\Psi^a_{FF}(x,t_0+\Delta t)\approx\Psi^a_{FF}(x,t_0)-\frac{i}{\hbar}\Delta t\{\frac{-\hbar^2}{2m}\frac{\partial^2\Psi^a_{FF}(x,t_0)}{\partial x^2}+V^a_{FF}(x,t_0)\Psi^a_{FF}(x,t_0)\} \\ =\Psi_{FF}(x,t_0)-\frac{i}{\hbar}\Delta t\{\frac{-\hbar^2}{2m}\frac{\partial^2\Psi_{FF}(x,t_0)}{\partial x^2}+(V_{FF}(x,t_0)+\Delta V(x,t_0))\Psi_{FF}(x,t_0)\} \quad (3.7) \\ \approx\Psi_{FF}(x,t_0+\Delta t)-\frac{i}{\hbar}\Delta t\Delta V(x,t_0)\Psi_{FF}(x,t_0).$$

For a small Δt, we can use (3.7) to approximate $\Psi^a_{FF}(x,t_0+\Delta t)$ if the difference between $\Psi^a_{FF}(x,t)$ and $\Psi_{FF}(x,t)$ is small enough within the time interval between t_0 and $t=t_0+\Delta t$.

Using (3.7), we obtain

$$|\Delta\Psi_{FF}(x,t)|=|\Psi^{a}_{FF}(x,t)-\Psi_{FF}(x,t)|\propto R(x,\Lambda(t))|\Delta V(x,t)|, \tag{3.8}$$

for small $|\Delta\Psi_{FF}(x,t)|$. The important observation here is that, as $R(x,\Lambda(t))$ is getting smaller, bigger ΔV is acceptable.

This analysis shows that we have some freedom to choose the value of the applied potential $V^{a}_{FF}(x,t)$ as $R(x,\Lambda(t))\to 0$. Hence one possible solution to the indeterminacy problem is to assign an arbitrary finite value to $V_{FF}(x,t)$ in the region where $R(x,\Lambda(t))\to 0$ such that the potential will be smooth in space. This is the approach that we use.

From (3.6) and by using the definition of $\Delta V(x,t)=V^{a}_{FF}(x,t)-V_{FF}(x,t)$, we obtain

$$\begin{aligned}\Delta V(x.t)&=V^{a}_{FF}(x,t)-V_{0}(x,\Lambda(t))\\&\quad+\hbar\theta(x,\Lambda(t))\frac{\partial\alpha}{\partial t}+(\alpha^{2}(t)-1)\frac{\hbar^{2}}{2m}\frac{1}{R(x,\Lambda(t))}\frac{\partial^{2}R(x,\Lambda(t))}{\partial x^{2}}.\end{aligned} \tag{3.9}$$

Inserting (3.9) into (3.8) , we obtain

$$|\Delta\Psi_{FF}(x,t)|\propto\left|\hbar R(x,\Lambda(t))\theta(x,\Lambda(t))\frac{\partial\alpha}{\partial t}+(\alpha^{2}(t)-1)\frac{\hbar^{2}}{2m}\frac{\partial^{2}R(x,\Lambda(t))}{\partial x^{2}}\right|, \tag{3.10}$$

as $R(x,\Lambda(t))\to 0$.

There are two important points that are shown by (3.9) and (3.10):

1. We require that $|\Delta\Psi_{FF}(x,t)|\to 0$ as $R(x,\Lambda(t))\to 0$. Hence, we should have $\left|\frac{\partial^{2}R(x,\Lambda(t))}{\partial x^{2}}\right|\to 0$ and $R(x,\Lambda(t))\theta(x,\Lambda(t))\to 0$ as $R(x,\Lambda(t))\to 0$ in order to be able to apply the Fast-Forward technique.
2. The error, $|\Delta\Psi_{FF}(x,t)|$, grows quadratically with the magnification factor α .

Though we use (3.6) to obtain the two points above, these are also true for the other formulations of the fast-forward potential as they are all equivalent.

In terms of implementation, the form of $V_{FF}(x,t)$ in (3.5) is more convenient. First of all, it only depends on one variable; that is $\theta(x,t)$. Hence, we have fewer sources of error. Secondly, compared to the other forms of $V_{FF}(x,t)$ where second order derivatives are needed, only first order derivatives in space and time are used in (3.5). Since it is easier to get higher accuracy for lower order derivatives, equation (3.5) is more preferable than the other forms of $V_{FF}(x,t)$.

Due to these reasons, we choose (3.5) to calculate $V_{FF}(x,t)$. For the region where $R(x,\Lambda(t))$ is small (i.e. $R(x,\Lambda(t))\le R_{\min}$), we model $\theta(x,\Lambda(t))$ using a polynomial of order 3 such that at the boundaries of this region, the values of $\frac{\partial\theta(x,\Lambda(t))}{\partial x}$ and $\theta(x,\Lambda(t))$ are matched with the ones obtained from the simulation. At the boundaries of the simulated space, we assign $\frac{\partial\theta(x,\Lambda(t))}{\partial x}=0$ and disregard the value of $\theta(x,\Lambda(t))$ obtained from the simulation. By doing numerical simulations, we find that the value of $R_{\min}=10^{-2.9}$ gives relatively good results.

In this project, the following equation is used for the magnification factor:

$$\alpha(t)=\alpha_m-(\alpha_m-1)\cos(\frac{2\pi t}{T_f}), \tag{3.11}$$

where $\alpha_m=\frac{T_0}{T_f}$, T_f is the duration of the accelerated quantum dynamics and, T_0 is the initial quantum dynamics duration.

3.1.3. Shortcut to adiabaticity

The main problem with accelerating an adiabatic process is that the time needed for an adiabatic process, by definition, is infinite. Accelerating an adiabatic process such that only finite time is needed means that an infinitely large magnification factor has to be used. It was shown in [10] that the fact that the phase of an adiabatic wave function has an infinitely small variation in space such that the product between this variation and the magnification factor can give a finite quantity can be used to handle this problem.

Here we will derive the expression of the fast-forward potential in the case where the initial quantum dynamics is an adiabatic process. We use $\Psi_0(x,t)\approx|\phi(x,t)|e^{i\theta(x,t)}$ where

$$\frac{-\hbar^2}{2m}\frac{\partial^2\phi(x,t)}{\partial x^2}+V_0(x,t)\phi(x,t)=E\phi(x,t)$$

and $\phi(x,t)$ is real. It is possible to approximate $\Psi_0(x,t)$ using this form because, by definition, the wave function of an adiabatic process follows one of the eigenstates of the time-dependent Hamiltonian which we denote as $\phi(x,t)$.

We can write the phase of $\Psi_0(x,t)$ as $\theta(x,t)=\theta_a(t)+\epsilon\delta(x,t)+k\pi$, where $\epsilon\to 0$ and k is 0 when $\phi(x,t)=|\phi(x,t)|$ and 1 otherwise. The term $\theta_a(t)$ is related to the time evolution of the eigenstate of the time-dependent Hamiltonian and to the geometric phase [15]. Except at the position where $\lim_{x\to x^-} sgn(\phi(x,t))\neq\lim_{x\to x^+} sgn(\phi(x,t))$, the last term, $k\pi$, can be considered as a space-independent term. It is necessary that $\phi(x,t)=0$ at the position where its sign changes. From our discussion in section 3.1.2, we know that the values of $V_{FF}(x,t)$ at the positions where $\phi(x,t)=0$ are not important. Hence, this last term can just be considered as a space-independent term.

Using (3.5) and the expression of $\theta(x,t)$ described above, we obtain

$$\begin{aligned} V_{FF}(x,t)=&V_0(x,\Lambda(t))-\hbar\delta(x,\Lambda(t))\epsilon\frac{\partial\alpha}{\partial t}\\ &-(\alpha^2(t)-1)\{\hbar\epsilon\frac{\partial\delta(x,t')}{\partial t'}|_{t'=\Lambda(t)}+\frac{\hbar^2\epsilon^2}{2m}(\frac{\partial\delta(x,\Lambda(t))}{\partial x})^2\}, \end{aligned} \tag{3.12}$$

after ignoring the space-independent terms. The reason why we can neglect the space-independent terms is because the space-independent potential only contributes to an additional space-independent phase to the final wave function. In many cases such as transport, a space-independent phase is not important.

Next, we assume that $\delta_1(x,r(\Lambda(t)))$ can be found such that $\delta_1(x,r(\Lambda(t)))=\delta(x,\Lambda(t))$ and $\frac{dr(t)}{dt}=\epsilon$. This means that we can write $\frac{\partial\delta}{\partial t}$ as $\frac{\partial\delta}{\partial t}=\frac{dr}{dt}\frac{\partial\delta_1}{\partial r}=\epsilon\frac{\partial\delta_1}{\partial r}$. Using this in (3.12), we obtain

$$V_{FF}(x,t)=V_0(x,\Lambda(t))-\hbar\,\delta_1(x,r(\Lambda(t)))\frac{\partial(\alpha\epsilon)}{\partial t}$$
$$-((\alpha\epsilon)^2(t)-\epsilon^2)\{\hbar\frac{\partial\delta_1(x,r')}{\partial r'}|_{r'=r(\Lambda(t))}+\frac{\hbar^2}{2m}(\frac{\partial\delta_1(x,r(\Lambda(t)))}{\partial x})^2\}. \quad (3.13)$$

Next, by neglecting the terms with only ϵ^2 dependence, we obtain the final expression of $V_{FF}(x,t)$ as

$$V_{FF}(x,t)=V_0(x,\Lambda(t))-\hbar\,\delta_1(x,r(\Lambda(t)))\frac{\partial(\alpha\epsilon)}{\partial t}$$
$$-(\alpha\epsilon)^2(t)\{\hbar\frac{\partial\delta_1(x,r')}{\partial r'}|_{r'=r(\Lambda(t))}+\frac{\hbar^2}{2m}(\frac{\partial\delta_1(x,r(\Lambda(t)))}{\partial x})^2\}. \quad (3.14)$$

This expression is similar to the expression of $V_{FF}(x,t)$ in equation (2.28) in [10]. The difference is that there is one term missing in (3.14). This is because we use $\theta(x,t)=\gamma(t)+\epsilon\delta(x,t)$ which means that there is no space-dependent term of order $O(1)$ in the eigenfunction of the time-dependent Hamiltonian. In this case, $V_{FF}(x,t)$ described by (3.14) will exactly be the same as $V_{FF}(x,t)$ described by equation (2.28) in [10]. Since we only deal with the case where $V_0(x,t)$ is real, it is always possible to obtain a real eigenfunction which means there is no space-dependent term of order $O(1)$ in the eigenfunction. Hence, (3.14) will be sufficient for our purpose.

From (3.14), we can see that, in the case of the fast-forwarding of an adiabatic process, instead of specifying $\alpha(t)$ we can specify $(\alpha\epsilon)(t)$. This $(\alpha\epsilon)(t)$ is finite due to the fact that, while $\alpha(t)$ is infinitely large, $|\epsilon|$ is infinitely small.

The next problem is to find the expression of $\delta_1(x,r)$. As it has been shown in [10], we can use the continuity equation in order to do this. Applying the continuity equation to $\Psi_0(x,t)$ we obtain

$$\frac{\partial}{\partial x}\{\phi^2\frac{\partial(\epsilon\,\delta(x,t)+k\,\pi)}{\partial x}\}=\frac{-m}{\hbar}\frac{\partial\phi^2}{\partial t}. \quad (3.15)$$

We can divide the space into some separated regions where the value of $sgn(\phi(x,t))$ is constant in each region. In one of these regions, (3.15) can be written as

$$\frac{\partial}{\partial x}\{\phi^2\frac{\partial\delta(x,t)}{\partial x}\}=-\frac{m}{\epsilon\hbar}\frac{\partial\phi^2}{\partial t}. \quad (3.16)$$

Next, assume that $\phi_1(x,r(t))$ can be found such that $\phi_1(x,r(t))=\phi(x,t)$ and $\frac{dr(t)}{dt}=\epsilon$. Using $\phi_1(x,r(t))$ instead of $\phi(x,t)$ and $\delta_1(x,r(t))$ instead of $\delta(x,t)$ in (3.16), we obtain

$$\phi_1^2\frac{\partial^2\delta_1}{\partial x^2}+2\phi_1\frac{\partial\phi_1}{\partial x}\frac{\partial\delta_1}{\partial x}+\frac{2m}{\hbar}\phi_1\frac{\partial\phi_1}{\partial r}=0. \quad (3.17)$$

Equation (3.17) is the same as equation (2.18) in [10]. By solving (3.17) we can obtain $\delta_1(x,r)$ for each regions where the value of $sgn(\phi(x,t))$ is constant. Hence, we have obtained the same results as the ones presented in [10].

Note that in deriving (3.17) we have used $\Psi_0(x,t)\approx|\phi(x,t)|e^{i\theta(x,t)}$ in the continuity equation. As it has been shown in [10], this is acceptable because this approximation of $\Psi_0(x,t)$ satisfies the Schrödinger equation up to $O(\epsilon)$. However, this approximation can not be applied if we use (3.6) to calculate the fast-forward potential. It can be shown that using this approximation in (3.6)

will lead to contradictory results. One example of such contradiction is shown in Appendix C.

There are some cases where it is difficult or impossible to find $\phi_1(x,r(t))$ such that $\phi_1(x,r(t))=\phi(x,t)$ and $\frac{dr(t)}{dt}=\epsilon$. For these cases, instead of trying to find $\delta_1(x,r)$, we can try to find the expression of $\delta(x,t)$ by solving (3.16) directly.

The problem is that the right hand side of equation (3.16) contains a division by ϵ and we know that $\epsilon\to 0$. In order to handle this, we use $\epsilon=\frac{1}{T_0}$, where T_0 is the time needed by the adiabatic process and we assume that any time derivative is in the order of $O(\frac{1}{T_0})$. Hence, we can rewrite (3.16) as

$$\frac{\partial}{\partial x}\{\phi^2\frac{\partial\delta(x,t)}{\partial x}\}=-\frac{m}{\hbar}\{T_0\frac{\partial\phi^2}{\partial t}\}, \tag{3.18}$$

which is solvable if $T_0\frac{\partial\phi^2}{\partial t}$ is finite. By solving this equation we can find $\delta(x,t)$ for each of the regions where the value of $sgn(\phi(x,t))$ is constant.

Since we use $\delta(x,t)$ instead of $\delta_1(x,r)$ we can not use (3.14) to calculate the fast-forward potential. However, by using $\epsilon=\frac{1}{T_0}$ and assuming that $T_0\frac{\partial\delta(x,t)}{\partial t}$ is finite, we can use (3.12) to obtain

$$\begin{aligned}V_{FF}(x,t)=V_0(x,\Lambda(t))-\hbar\delta(x,\Lambda(t))\frac{\partial(\alpha\epsilon)}{\partial t}\\ -(\alpha\epsilon)^2(t)\{\hbar T_0\frac{\partial\delta(x,t')}{\partial t'}|_{t'=\Lambda(t)}+\frac{\hbar^2}{2m}(\frac{\partial\delta(x,\Lambda(t))}{\partial x})^2\}.\end{aligned} \tag{3.19}$$

Here, we have neglected the terms with ϵ^2 dependence.

There is still one remaining problem. As it has been stated before, both (3.17) and (3.18) can only be used for separated regions where $sgn(\phi(x,t))$ is constant in each region. The problem is how to connect the solution between one region and the other. Here, we will present a solution to this problem.

From (3.18) we obtain

$$\phi^2\frac{\partial\delta(x,t)}{\partial x}=-\frac{m}{\hbar}\int dx\{T_0\frac{\partial\phi^2}{\partial t}\}. \tag{3.20}$$

Note that the right hand side of (3.20) is an indefinite integral. The left hand side of (3.20) has to be equal to 0 if $\phi(x,t)=0$. Hence, it is correct to write

$$\phi^2(x,t)\frac{\partial\delta(x,t)}{\partial x}=-\frac{m}{\hbar}\int_{x_0(t)}^{x}dx'\{T_0\frac{\partial\phi^2(x',t)}{\partial t}\}, \tag{3.21}$$

with $\phi(x_0(t),t)=0$. In this way we do not have to worry about connecting two regions separated by $x_0(t)$ that have different value of $sgn(\phi(x,t))$. This is because equation (3.21) is correct for both regions.

We have not proved that the value of $\frac{\partial\delta(x,t)}{\partial x}$ will be finite around $x_0(t)$. It was shown in Section IV.C of [12] that this is indeed the case. Here we will follow similar arguments as in [12] to

show it.

Let us consider $\phi(x_0(t),t)=0$. Around $x_0(t)$ we can write

$$\phi(x,t)\approx\frac{\partial\phi(x,t)}{\partial x}|_{x_0(t)}(x-x_0(t))=W(t)(x-x_0(t)). \tag{3.22}$$

By using (3.22) in (3.21) and solving the integral at the right hand side of (3.21), we obtain

$$W^2(t)(x-x_0(t))^2\frac{\partial\delta(x,t)}{\partial x}=-\frac{m}{\hbar}T_0\{\frac{\partial W^2(t)}{\partial t}\frac{(x-x_0(t))^3}{3}-\frac{\mathrm{d}x_0}{\mathrm{d}t}W^2(t)(x-x_0(t))^2\}, \tag{3.23}$$

$$\frac{\partial\delta(x,t)}{\partial x}=-\frac{m}{\hbar}T_0\{\frac{\partial W^2(t)}{\partial t}\frac{(x-x_0(t))}{3W^2(t)}-\frac{\mathrm{d}x_0}{\mathrm{d}t}\}. \tag{3.24}$$

As can be seen from (3.24), $\frac{\partial\delta(x,t)}{\partial x}$ is finite around $x_0(t)$.

However, there is a fault in this reasoning. We assume that (3.21) is true. However, equation (3.21) is only true if

$$\int_{x_i(t)}^{x_j(t)}\mathrm{d}x'\{T_0\frac{\partial\phi^2(x',t)}{\partial t}\}=0, x_{i,j}(t)\in\{x(t)|\phi(x(t),t)=0\}. \tag{3.25}$$

If this condition is not satisfied then there is no finite solution for $\frac{\partial\delta(x,t)}{\partial x}$.

The discussion above applies for $x\in]-\infty,\infty[$. If we disregard relativity, there is no reason to impose $\frac{\partial\delta(x,t)}{\partial x}$ to be finite for $x\in\{-\infty,\infty\}$ since we will not be able to control the potential at these positions anyway. However, in order for the potential to be realizable, we can impose that $\phi^2(x,t)\frac{\partial\delta(x,t)}{\partial x}=0$ for $x\in\{-\infty,\infty\}$. In this way the potential gradient in space will not be very large. If we impose this condition, we can obtain

$$\int_{-\infty}^{x_0(t)}\mathrm{d}x'\{T_0\frac{\partial\phi^2(x',t)}{\partial t}\}=0,\forall x_0(t)\in\{x(t)|\phi(x(t),t)=0\}, \tag{3.26}$$

as a requirement that has to be fulfilled for a realizable shortcut to adiabaticity.

Given that (3.26) is satisfied, equation (3.24) can be used to calculate $\frac{\partial\delta(x,t)}{\partial x}$ in the vicinity of $x_0(t)$ where $\phi(x_0(t),t)=0$. For the regions where $\phi(x,t)$ is big enough, (3.18) can be solved numerically with the boundary condition is calculated using (3.24). In the case where there are more than one nodes, $\frac{\partial\delta(x,t)}{\partial x}$ is guaranteed to be continuous if (3.26) is satisfied. Similar arguments can also be applied for the case where, instead of $\delta(x,t)$, $\delta_1(x,r)$ is used.

The main advantage of the shortcut to adiabaticity is that we do not depend on the magnification factor at all. Hence, in general, it is more preferable to work with the shortcut to adiabaticity. However, the normal Fast-Forward technique has some advantages in terms of its versatility. In some cases when it is difficult to get an analytical expression of the system's eigenstate or when equation (3.26) is not satisfied, we can still use the normal Fast-Forward technique to speed up the quantum dynamics of the process.

We derive the magnification factor used for the shortcut to adiabaticity from (3.11) as below

$$\begin{aligned}\alpha(t)\epsilon &= \lim_{T_0\to\infty}\{\alpha_m-(\alpha_m-1)\cos(\frac{2\pi t}{T_f})\}\frac{1}{T_0}\\ &=\frac{1}{T_f}(1-\cos(\frac{2\pi t}{T_f})).\end{aligned} \tag{3.27}$$

The parameter $\Lambda(t)$ related to this magnification factor can be calculated as

$$\begin{aligned}\frac{\Lambda(t)}{T_0} &= \int_0^t \mathrm{d}\,t'\alpha(t')\epsilon\\ &= \frac{t}{T_f}-\frac{1}{2\pi}\sin(\frac{2\pi t}{T_f}).\end{aligned} \tag{3.28}$$

3.2. Adiabatic translation of a single neutral atom in a harmonic trap

We consider the case where a single neutral atom is in the ground state of a harmonic trap. We would like to move this trap while maintaining the atom in the ground state. This can be done by moving the harmonic trap adiabatically. The potential, $V_0(x,t)$, can be written as:

$$V_0(x,t)=\frac{\hbar\omega}{2L^2}(x-x_c(t))^2, \tag{3.29}$$

where $x_c(t)$ is the time-dependent position of the center of the trap. Initially, the atom is in the ground state of this potential and the ground state's eigenfunction is given by $\Phi_0(x-x_c(0))$ where $\Phi_n(x)$ is given in (2.3a).

The adiabaticity condition for this case can be written as (see Appendix B):

$$\left|\frac{\mathrm{d}\,x_c}{\mathrm{d}\,t}\right|\le 0.1\,\omega\,L. \tag{3.30}$$

As an example, we use the trap velocity,

$$\frac{\mathrm{d}\,x_c}{\mathrm{d}\,t}(t)=\frac{v_{max}}{2}\{1-\cos(\frac{2\pi t}{T})\}, \tag{3.31}$$

with the maximum speed, v_{max}, related to the maximum displacement, x_{max}, by $v_{max}=\frac{2x_{max}}{T}$. In order to fulfill (3.30), we impose $v_{max}=0.1\,\omega\,L$. In our example, we use $x_{max}=3L$. Hence, to fulfill the adiabaticity condition, $T\ge\frac{60}{\omega}$ is needed.

We would like to speed up this transport 10 times from $T_0=\frac{60}{\omega}$ to $T_f=\frac{6}{\omega}$. The simulation result of the transport using $T=\frac{60}{\omega}$ and $T=\frac{6}{\omega}$ (before fast-forwarding) is shown in Figure 13(a) and 13(b), respectively. The simulation result of the transport using $T=\frac{6}{\omega}$ after applying the Fast-Forward technique is shown in Figure 14. From Figure 13 and 14, we can see that the Fast-Forward technique has been successfully implemented.

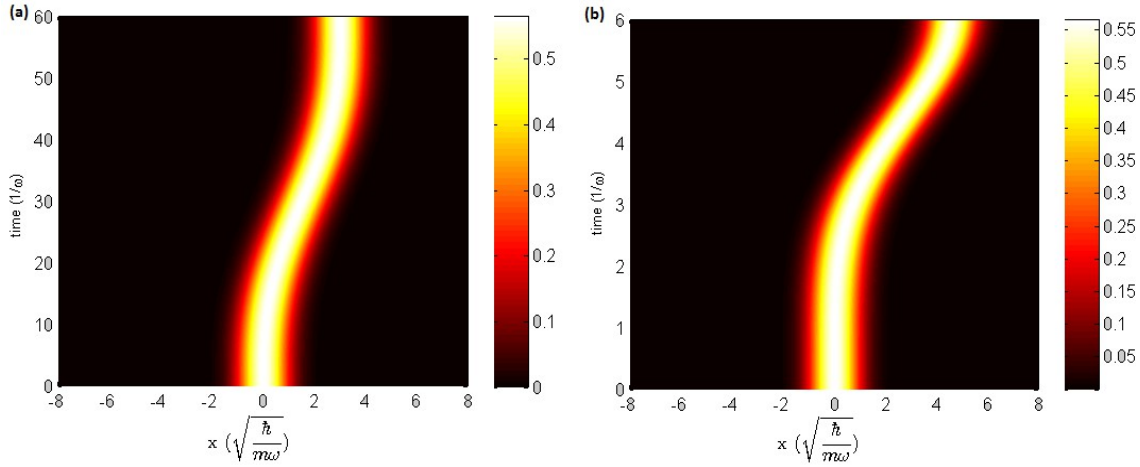

Figure 13. Spatio-temporal evolution of the probability density during the transport of a single neutral atom with $T=\frac{60}{\omega}$ (a) and with $T=\frac{6}{\omega}$ (before fast-forwarding) (b) . The value $x_{max}=3L$ is used in both cases.

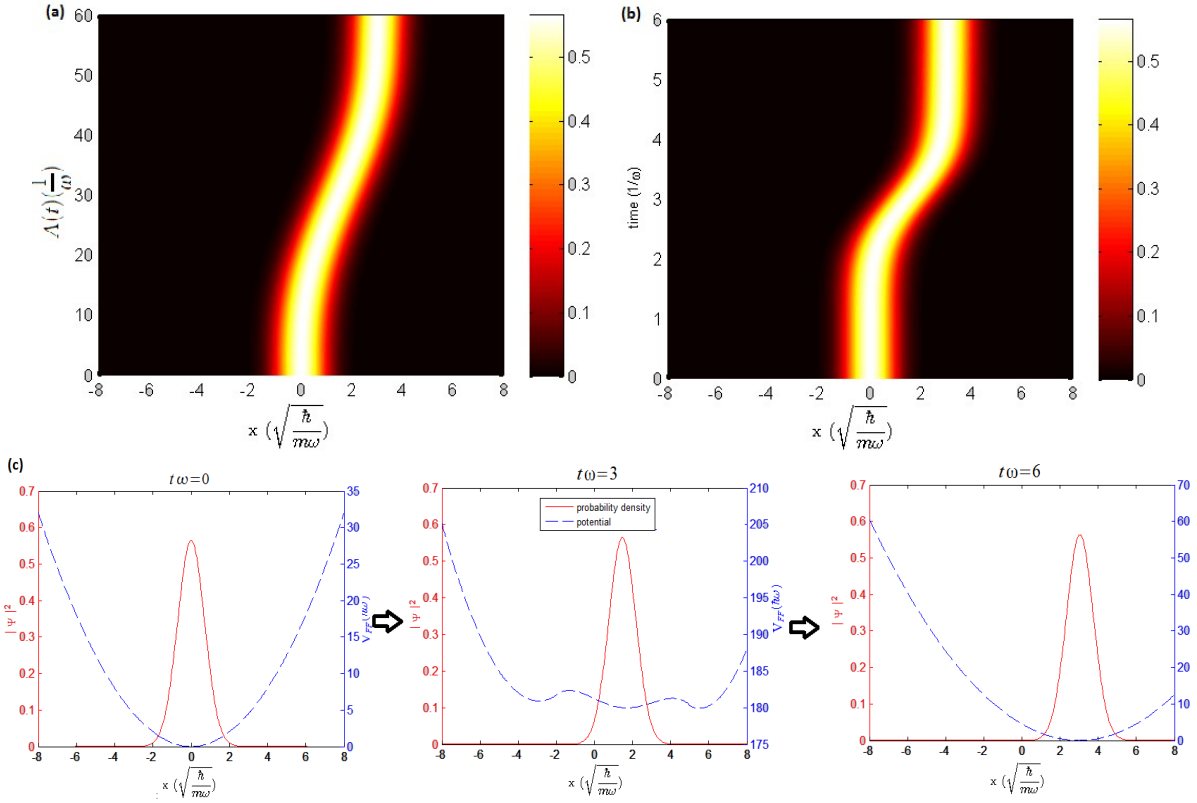

Figure 14. Spatio-temporal evolution of the probability density during the transport of a single neutral atom with $T_f=\frac{6}{\omega}$ (after fast-forwarding) and $T_0=\frac{60}{\omega}$. In (a), the plot against the fast-forwarded time $\Lambda(t)$ is shown, while in (b), normal time (t) is used. The snapshots of the fast-forwarded potential and the probability density at three different times are shown in (c). The value $x_{max}=3L$ is used.

In order to evaluate the accuracy of the Fast-Forward technique, we calculate the fidelity which is defined as $F(t)=\left|\langle\Psi_{ff}(t)|\Psi_0(\Lambda(t))\rangle\right|$. The plot of the time evolution of the fidelity is shown in Figure 15. Here, we see that initially the fidelity is 1. It decreases and then increases afterwards until it reaches a very close value to 1 at the final time. This is expected since during the fast-

forwarding we introduce an additional phase to the wave function. This additional phase reduces to zero as we approach the final time.

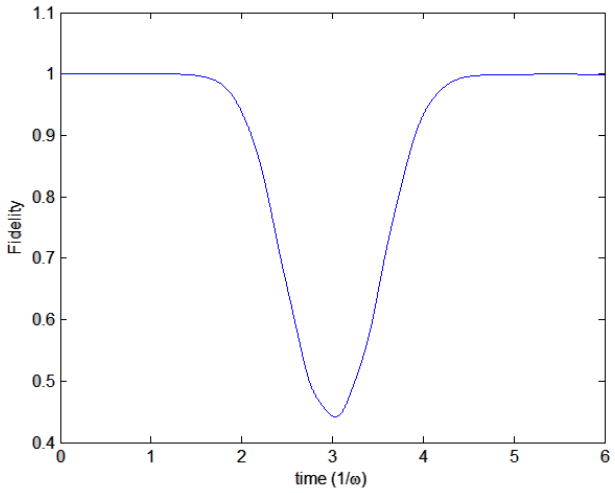

Figure 15. Time evolution of the fidelity for the fast-forwarding of the transport of a single neutral atom. The parameters used are as in Figure 14.

For the case of the adiabatic translation, it is possible to formulate a shortcut to adiabaticity based on the Fast-Forward technique. Let us consider $V_0(x,t)=V_{00}(x-x_c(t))$ where $V_{00}(x)$ is the potential at the initial time. In this case, $\phi(x,t)=\phi_{00}(x-x_c(t))$ where $\phi_{00}(x)$ is the eigenstate at the initial time. Using this $\phi(x,t)$ in equation (3.18) we obtain

$$\begin{aligned}\delta(x,t)&=-\frac{m}{\hbar}T_0\int_0^x \mathrm{d}x_1\frac{1}{\phi^2(x_1,t)}\int_{-\infty}^{x_1}\mathrm{d}x_2\frac{\partial\phi^2(x_2,t)}{\partial t}\\&=-\frac{m}{\hbar}T_0\int_0^x \mathrm{d}x_1\frac{1}{\phi_{00}^2(x_1-x_c(t))}\int_{-\infty}^{x_1}\mathrm{d}x_2\frac{\partial\phi_{00}^2(x_2-x_c(t))}{\partial t}\\&=\frac{m\dot{x}}{\hbar}T_0\frac{\mathrm{d}x_c}{\mathrm{d}t}.\end{aligned}\qquad(3.32)$$

Using (3.32) and by neglecting the space-independent terms we can obtain

$$V_{FF}(x,t)=V_{00}(x-x_c(\Lambda(t)))-m\dot{x}\{\{T_0\frac{\mathrm{d}x_c}{\mathrm{d}t}|_{\Lambda(t)}\}\frac{\partial(\alpha\epsilon)}{\partial t}+\{T_0^2\frac{\mathrm{d}^2x_c}{\mathrm{d}t^2}|_{\Lambda(t)}\}(\alpha\epsilon)^2\}\quad.\qquad(3.33)$$

Equation (3.33) is valid for any potential $V_{00}(x)$ and any eigenstate related to this potential. Up to irrelevant additional space-independent terms, equation (3.11) in [10] coincides with equation (3.33) when $\frac{\mathrm{d}x_c}{\mathrm{d}t}=\frac{1}{T_0}$ or, in other words, when the trap moves with constant velocity.

In the example presented here, $V_{00}(x)$ is equal to $V_0(x,0)$, where $V_0(x,t)$ is given in (3.29) . Initially, the atom is in the ground state of this potential. The parameter $\alpha\epsilon$ is given in equation (3.27). We use (3.31) and (3.28) to obtain

$$T_0\frac{\mathrm{d}x_c(t')}{\mathrm{d}t'}|_{t'=\Lambda(t)}=x_{max}\{1-\cos(\frac{2\pi t}{T_f}-\sin(\frac{2\pi t}{T_f}))\}\quad\text{and}$$

$$T_0^2\frac{\mathrm{d}^2x_c(t')}{\mathrm{d}t'^2}|_{t'=\Lambda(t)}=2\pi x_{max}\sin(\frac{2\pi t}{T_f}-\sin(\frac{2\pi t}{T_f}))\quad.$$

The value of $x_{max}=3L$ is used. The results for $T_f=\frac{6}{\omega}$ and $T_f=\frac{1}{\omega}$ are shown in Figure 16(a) and 16(b), respectively. The fidelity of the transport in this case is defined as $F(t)=\left|\langle\Psi_{ff}(t)|\Phi_0(x-x_c(\Lambda(t)))\rangle\right|$. The plot of the time evolution of this fidelity is shown in Figure 17(a) and 17(b) for $T_f=\frac{6}{\omega}$ and $T_f=\frac{1}{\omega}$, respectively.

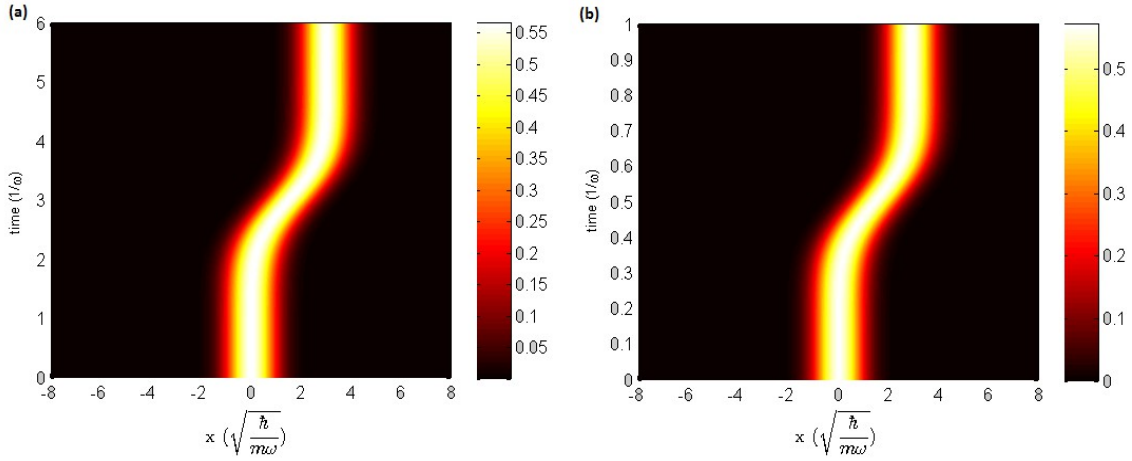

Figure 16. Spatio-temporal evolution of the probability density during the transport of a single neutral atom with $T_f=\frac{6}{\omega}$ (a) and $T_f=\frac{1}{\omega}$ (b) when shortcut to adiabaticity is used. The value $x_{max}=3L$ is used in both cases.

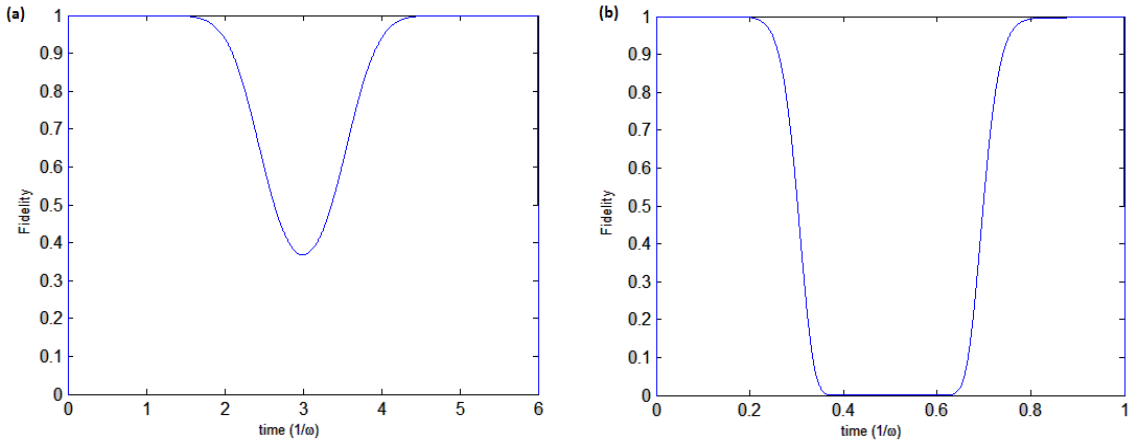

Figure 17. Time evolution of the fidelity for the transport of a single neutral atom utilizing shortcut to adiabaticity for $T_f=\frac{6}{\omega}$ (a) and $T_f=\frac{1}{\omega}$ (b). The parameters used are as in Figure 16.

From these results, we can see that one advantage of the shortcut to adiabaticity is that it is independent of the magnification factor α. Hence, the quantum dynamics can be achieved in any desired time.

3.3. Transport of a neutral atom between the two extreme traps of a triple-well potential

As it has been mentioned in Section 2.3, it is possible to transport a single neutral atom between the two extreme traps of a triple-well potential in a robust way by using TLAO-based transport. However, due to the adiabaticity condition, the time needed for this process is larger than the time needed for the tunneling-based transport.

In order to speed up this transport process, we implement the Fast-Forward technique. We would like to accelerate the transport process 3 times from $T_0=\frac{165}{\omega}$ to $T_f=\frac{55}{\omega}$. The simulation results of the transport using $T=\frac{55}{\omega}$ without applying the Fast-Forward technique are shown in Figure 18. The simulation results after applying the Fast-Forward technique are shown in Figure 19. The definition of the population in each trap is given in (2.20) with $x_{mid1}(t)$ and $x_{mid2}(t)$ being calculated for $V_0(x,\Lambda(t))$.

From Figure 18 and Figure 19, we can see that the Fast-Forward technique has been successfully implemented. After the Fast-Forward technique is applied, the transfer efficiency is improved from 36.23% to 99.8%. In order to evaluate the accuracy of the Fast-Forward technique, we calculate the fidelity defined as $F(t)=\left|\langle\Psi_{ff}(t)|\Psi_0(\Lambda(t))\rangle\right|$ with $|\Psi_{ff}(t)\rangle$ and $|\Psi_0(t)\rangle$ being the fast-forwarded and the normal state, respectively. The plot of the time evolution of the fidelity is shown in Figure 20. As it is shown, the fidelity at the final time is very close to 1.

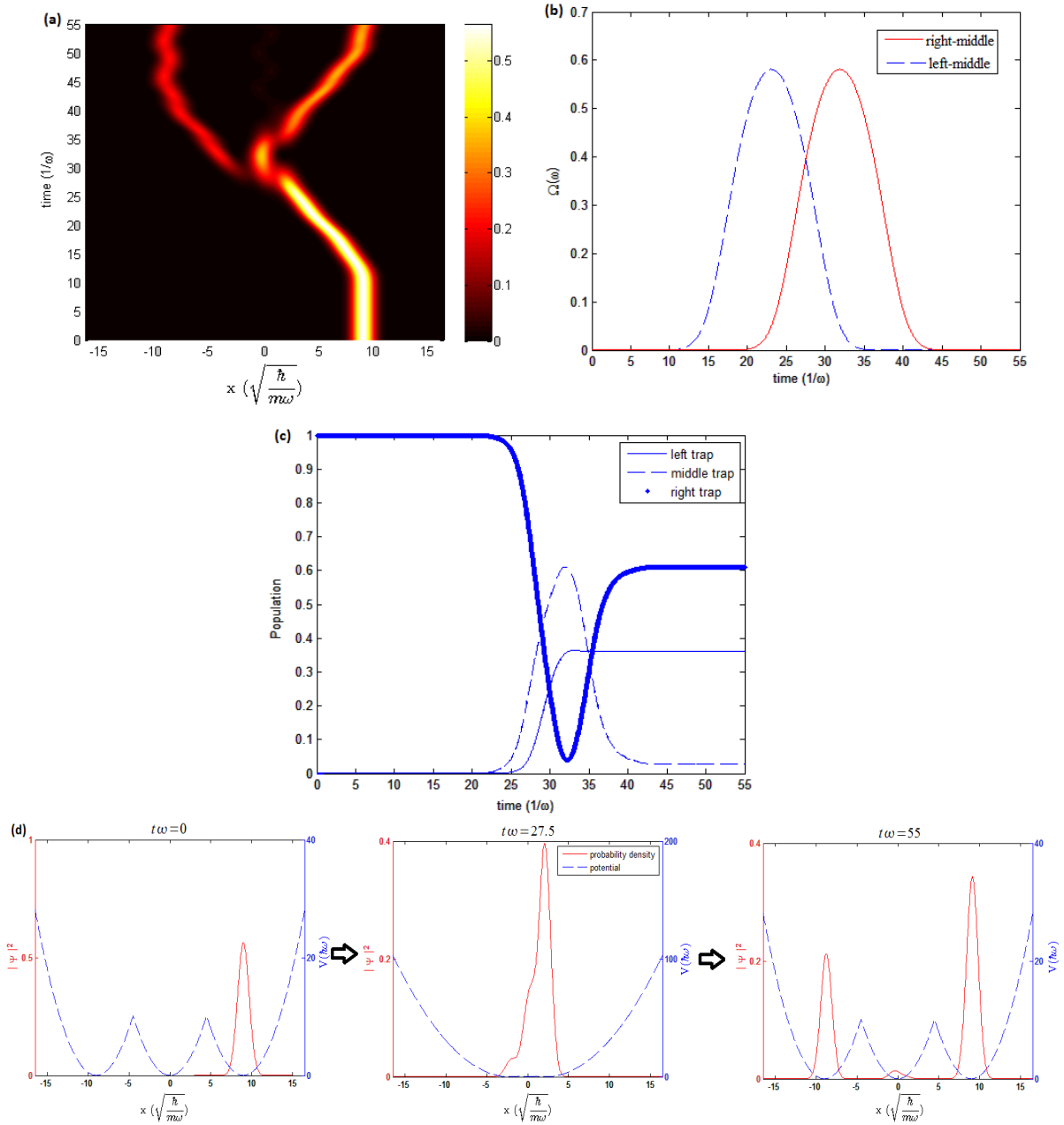

Figure 18. Simulation of the coherent population transfer of a single neutral atom between two traps using the usual TLAO-based transport for a total time, $T=\frac{55}{\omega}$ and pulse delay equal to $T_d=\frac{8.8}{\omega}$ that does not fulfill the adiabaticity condition. Here we show the spatio-temporal evolution of the probability density (a), the time evolution of the tunneling rate between the traps (b), the time evolution of the population in each trap (c), and the snapshots of the potential and the probability density at three different times (d). We use $18L$ as the initial and final distance.

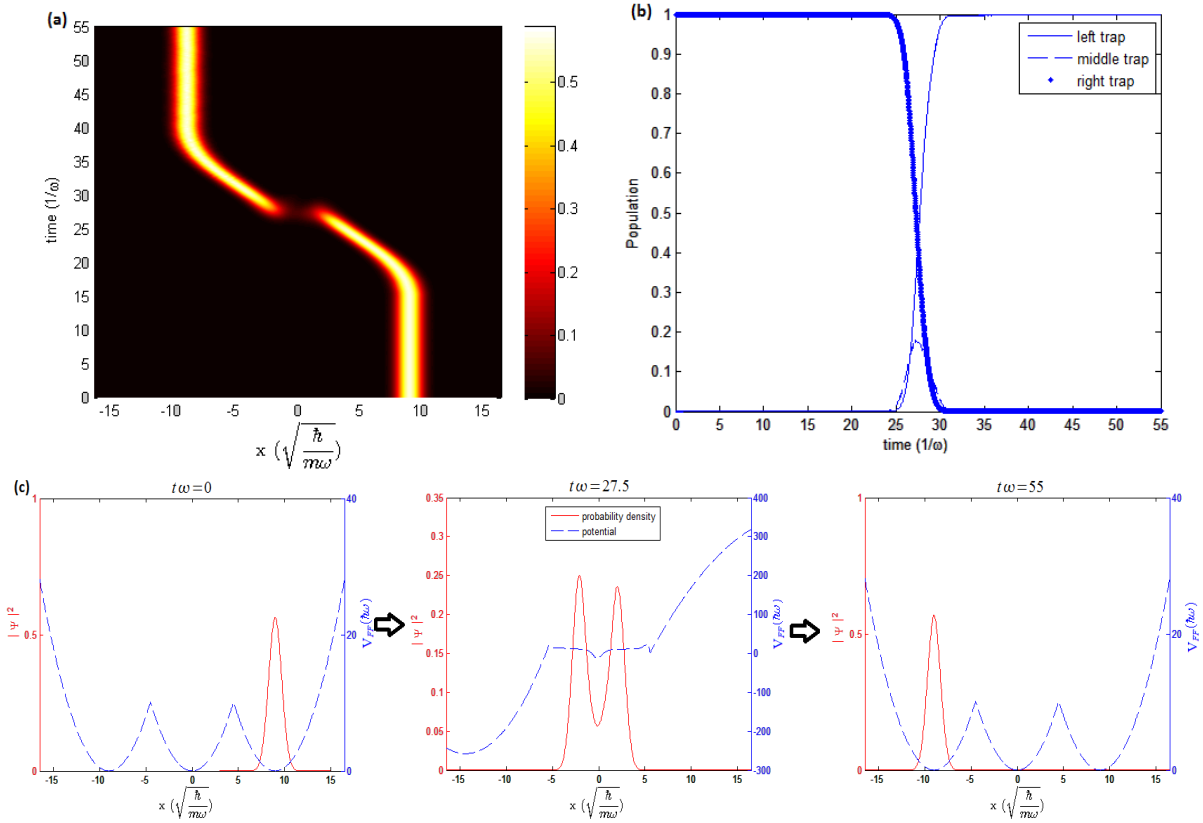

Figure 19. Simulation of the coherent population transfer of a single neutral atom between two traps using fast-forwarded TLAO-based transport with $T_f = \frac{55}{\omega}$ and $T_0 = \frac{165}{\omega}$. Here we show the spatio-temporal evolution of the probability density (a), the time evolution of the population in each trap (b), and the snapshots of the potential and the probability density at three different times (c). We use 18L as the initial and final distance.

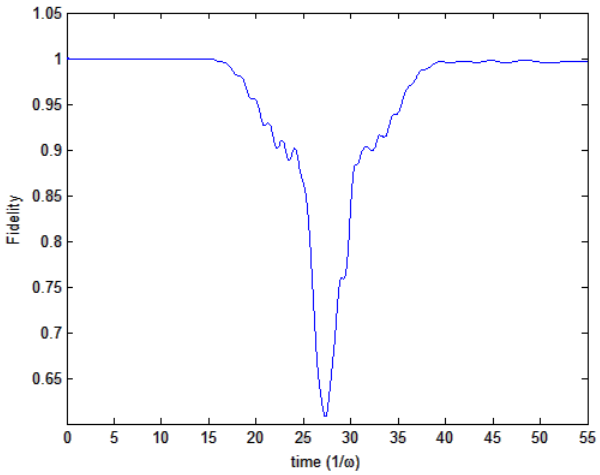

Figure 20. Time evolution of the fidelity for the fast-forwarding of the TLAO-based transport of a single neutral atom. The parameters used are as in Figure 19.

Next, we may ask if it is possible to create a shortcut to adiabaticity for the TLAO-based transport. We will show here that, under a certain reasonable assumption, it is not possible to create this shortcut using the Fast-Forward technique.

We approach this problem from two points of view. The first one is from the Bohmian mechanics

point of view. As it has been mentioned in Section 3.1.1, from the point of view of Bohmian mechanics, what the Fast-Forward technique does is to increase the trajectory velocity. However, as it has been shown in [27], if we use non-relativistic quantum mechanics, the trajectory velocity in the middle trap approach infinite as we approach the perfect adiabaticity.

There are two problems with this infinite trajectory velocity. First of all, since the expression of the fast-forward potential in equation (3.5) is proportional to the trajectory velocity, this gives a good indication that the resulted fast-forward potential will have a divergent point. Hence, the chance is high that it is not realizable. Secondly, the Fast-Forward theory described up to now is only valid if the relativistic effects can be neglected. The theory of relativity does not allow the trajectory velocity to be larger than the speed of light. This means that, in the perfect adiabaticity regime, relativistic quantum mechanics has to be used to describe the TLAO-based transport [27]. This indicates the need of incorporating relativity into the framework of the Fast-Forward technique. Up to now, this has not been done.

The arguments above give a good indication that it will be very difficult to derive a shortcut to adiabaticity for the TLAO-based transport using the Fast-Forward technique. However, it does not give a solid proof that it is impossible. One may argue that we can have a finite trajectory velocity if we allow the trajectory velocity at infinity to be infinite. Also, it is possible to argue that, although we do need to use relativistic quantum mechanics to describe the TLAO-based transport in the perfect adiabaticity regime, the Fast-Forward technique is applied in finite time regime. The adiabatic wave function only serves as a reference. Hence, the current Fast-Forward technique might be sufficient.

Our second approach is to evaluate equation (3.26).We will show that, if we impose equation (3.26) to be fulfilled for a fast-forward potential to be realizable, then it is impossible to derive a realizable shortcut to adiabaticity for the TLAO-based transport using the Fast-Forward technique.

In the perfect adiabaticity limit, the wave function in the TLAO-based transport with the atom in the right trap at the initial time can be written as

$$\phi(x,t)=a(t)\langle x|0;t\rangle(t)-b(t)\langle x|1;t\rangle, \tag{3.34}$$

where $\frac{b}{a}=\tan(\Theta)$, $|0\rangle$ and $|1\rangle$ are the ground state of the right trap and the left trap, respectively, and index *t* indicates that the parameters change with time since the position of the traps are time-dependent. The mixing angle, Θ , is defined as $\tan(\Theta)=\frac{\Omega_R}{\Omega_L}$ with Ω_R (Ω_L) being the tunneling rate between the right (left) trap and the middle trap. The values of *a* and *b* are chosen such that the normalization condition is fulfilled. The expression of the tunneling rate in Section 2.2 (see equation (2.12)) is used.

The expression for the integral in equation (3.26) can be solved analytically for the case of TLAO-based transport. We use (2.21a) and (2.21b) for the velocity of the traps. Figure 21(b) shows the plot of $S(\Lambda(t))=\{\int_{-\infty}^{x_0(t')} \mathrm{d}x'\{T_0\frac{\partial\phi^2(x',t')}{\partial t'}\}\}|_{t'=\Lambda(t)}$ with $\phi(x_0(\Lambda(t)),\Lambda(t))=0$ against fast-forwarded time, $\Lambda(t)$ for the case where the following parameters are used: minimum separation distance: $3.6L$, $x_{max}=14.4L$, and $T_d:T_1=4:21$. From this figure we can see that (3.26) is not fulfilled.

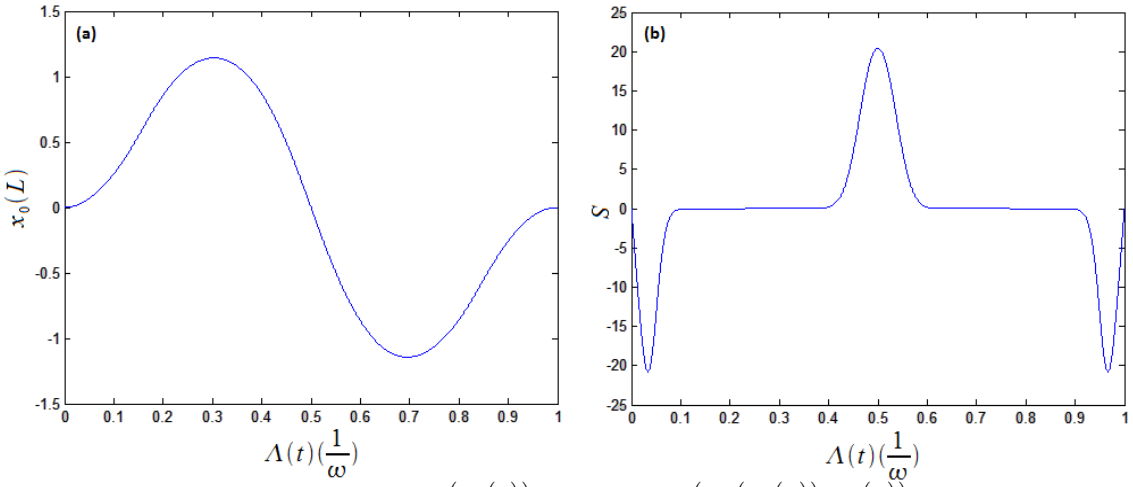

Figure 21. Temporal evolution of $x_0(\Lambda(t))$ where $\phi(x_0(\Lambda(t)),\Lambda(t))=0$ (a) and temporal evolution of $S(\Lambda(t))=\{\int_{-\infty}^{x_0(t')} \mathrm{d}x'\{T_0\frac{\partial\phi^2(x',t')}{\partial t'}\}\}|_{t'=\Lambda(t)}$ (b). The value of the minimum separation distance = 3.6L, $x_{max}=14.4L$, and $T_d:T_1=4:21$ are used.

Note that the argument using (3.26) is stronger than the one using Bohmian mechanics point of view. It is possible that (3.26) is fulfilled but the trajectory velocity of the adiabatic wave function exceeds the speed of light. One example of this case was presented in [12]. It was shown that it is possible to derive a realizable shortcut to adiabaticity for the case of adiabatic dilation although the value of the trajectory velocity, $S=\frac{\hbar}{m}\frac{\partial\delta}{\partial x}$, goes to infinity as $x\to\infty$. However, for this adiabatic dilation, equation (3.26) is still fulfilled.

As in the case of the TLAO-based transport and the tunneling-based transport discussed in Chapter 2, we conduct a robustness test for the fast-forwarded TLAO-based transport (with $T_f=\frac{55}{\omega}$, $T_0=\frac{165}{\omega}$) and compare it with the robustness of the TLAO-based transport (with $T=\frac{165}{\omega}$). The results are shown in Figure 22.

From Figure 22(a) and (b), we can see that for a wide range of shaking amplitudes and frequencies, both methods are robust but the fast-forwarded TLAO-based transport seems to be more robust than the usual TLAO-based transport. This is expected as the time needed by the the fast-forwarded TLAO-based transport is shorter. Hence, only shaking with high frequency will affect the fast-forwarded TLAO-based transport greatly.

Regarding the tilting of the experimental setup, from Figure 22(c) we can see that the fast-forwarded TLAO-based transport is more robust. The reason of this is because the fast-forward potential is dominated more by by high frequency components in space compared to the usual TLAO-based transport potential. Since the tilting affect mostly the lower frequency components, it affects the usual TLAO-based transport potential more than the fast-forwarded one.

Regarding the effect of the spatial and temporal resolution of the potential, the usual TLAO-based transport has higher transfer efficiency compared to the fast-forwarded one for the same values of the spatial and temporal resolution. This is also expected since the potential used in the usual TLAO-based transport has lower high frequency components, both in space and time.

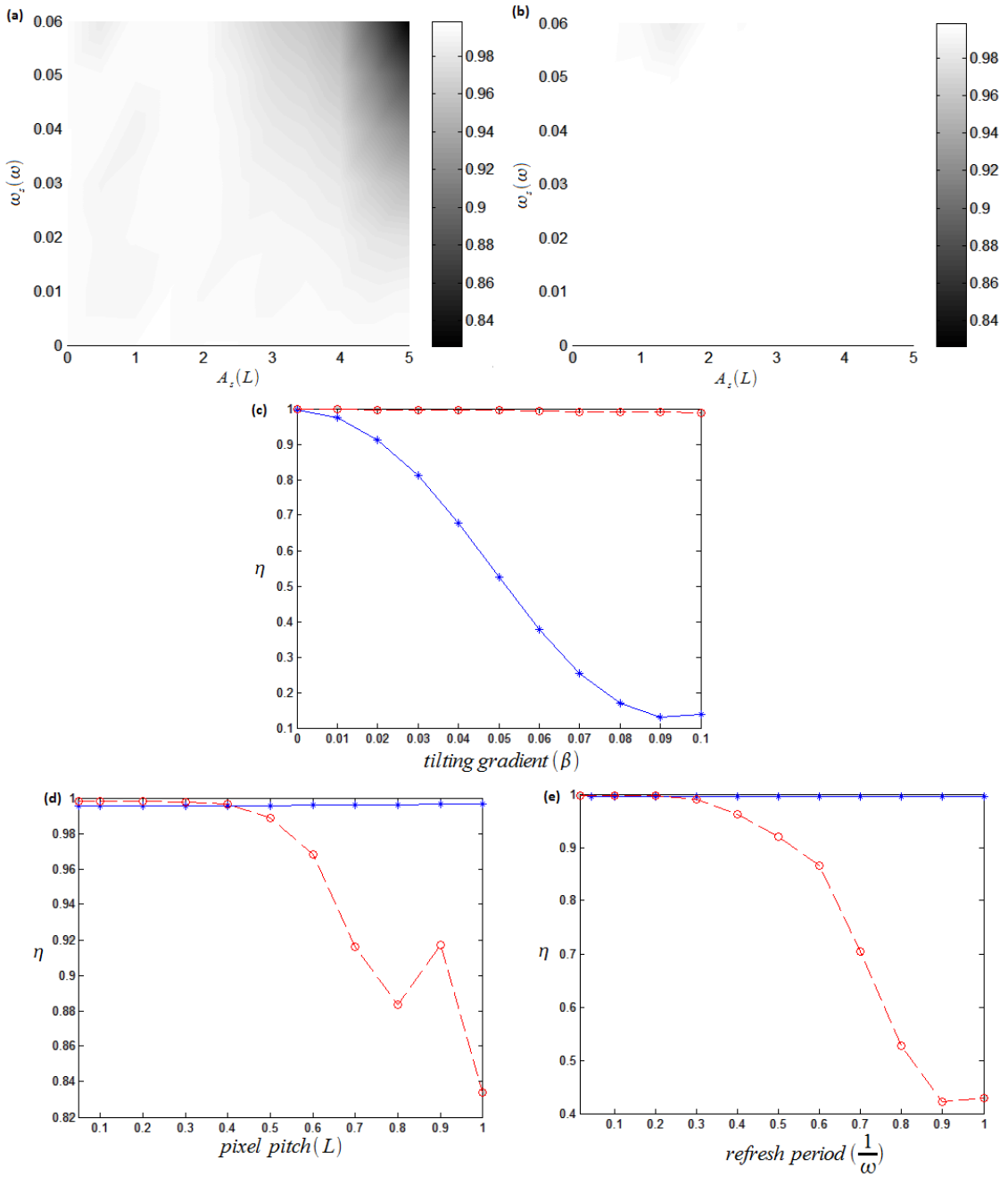

Figure 22. Comparison between the robustness of the usual and the fast-forwarded TLAO-based transport. Transfer efficiency of the usual (a) and the fast-forwarded (b) TLAO-based transport as a function of the shaking amplitude (A_s) and the shaking frequency (ω_s) are shown. In (c), (d), and (e), blue lines with star marks (—✳—) and red dashed lines with dot marks (—○—) represent the results for the case of the usual and the fast-forwarded TLAO-based transport, respectively. Transfer efficiency as a function of tilting gradient, β , is shown in (c). The effect of limited spatial and temporal resolution of the SLM are shown in (d) and (e), respectively.

As a conclusion, we have shown that it is possible to speed up the TLAO-based transport using the Fast-Forward technique though, under a reasonable assumption, it is not possible to derive a shortcut to adiabaticity for the TLAO-based transport using the Fast-Forward technique. For the set of parameters considered in this work, the resulted technique is more robust than the usual TLAO-based transport. However, it is more difficult to realize the fast-forward potential as it is less smooth compared to the potential in the usual TLAO-based transport which implies that a SLM with higher spatial resolution and refresh rate is needed.

CHAPTER FOUR
Conclusions

We have reviewed two techniques to transport a single neutral atom between two harmonic traps. The first one is the tunneling-based transport [3] and the second one is the Three-Level Atom Optics (TLAO) based transport [4]. The TLAO-based transport is more robust than the tunneling-based transport. However, it is slower due to the adiabaticity condition [3].

By implementing the Fast-Forward technique [11] to the TLAO-based transport, we have successfully obtained a faster transport technique while maintaining, or even improving for certain parameters, the robustness of the TLAO-based transport. Our implementation is based on the Fast-Forward technique described in [11] that can be applied to quantum dynamics of non-adiabatic processes. Hence, we only accelerated a nearly-adiabatic process instead of accelerating a fully adiabatic process. As a result, we have only obtained a transfer efficiency around 99% instead of 100% that is theoretically possible for an adiabatic processes.

We have studied the robustness of the resulted technique numerically. We have considered four possible experimental imperfections. They are shaking and tilting of the experimental setup, and limited pixel pitch and refresh rate of the potential. Our results show that the fast-forwarded TLAO-based transport is more robust than the TLAO-based transport against shaking and tilting of the experimental setup. The main problem with the fast-forwarded TLAO-based transport is regarding the high space and time resolution of the potential needed. The requirements for the resolution, both in space and time, are higher for the fast-forwarded TLAO-based transport than for the usual TLAO-based transport.

In some cases, it is possible to accelerate an adiabatic process (that is to create a shortcut to adiabaticity) by using the Fast-Forward technique described in [10]. We have used two approaches to find out if this is possible for the TLAO-based transport. The first one was to interpret the Fast-Forward technique from the point of view of Bohmian mechanics. From this point of view, the fast-forwarding of a quantum dynamics results in a faster trajectory velocity. However, as has been shown in [27], the trajectory velocity at the middle trap of a triple-well potential grows without bound in the TLAO-based transport. Our second approach was to give a mathematical condition for a realizable fast-forward potential. We showed that this condition can not be fulfilled for the case of the fast-forwarding of the TLAO-based transport.

Further research directions can include studying the fast-forwarding of the TLAO-based transport in a two-dimensional (2D) setup. Although it is more complicated, the extra space dimension gives more freedom. For example, it might be possible to use a 2D nearly time-independent potential instead of a 1D time-dependent potential by coupling the time dimension into one of the space dimensions. If this is possible, higher spatial resolution can be achieved by using a prefabricated mask instead of a SLM.

Another possible research direction is to apply other alternative techniques to obtain a shortcut to adiabaticity for the TLAO-based transport or to apply the Fast-Forward technique to other transport schemes. For example, a robust tunneling-based transport can be done if the minimum distance between the traps is large enough. However, this is a very slow process. We can apply Fast-Forward technique to speed up this process.

REFERENCES

[1] Frese, D., Ueberholz, B., Kuhr, S., Alt, W., Schrader, D., Gomer, V., & Meschede, D. (2000). Single atoms in an optical dipole trap: Towards a deterministic source of cold atoms. *Physical Review Letters*, 85(18), 3777.

[2] Puppe, T., Schuster, I., Grothe, A., Kubanek, A., Murr, K., Pinkse, P. W. H., & Rempe, G. (2007). Trapping and observing single atoms in a blue-detuned intracavity dipole trap. *Physical Review Letters*, 99(1), 013002.

[3] Mompart, J., Eckert, K., Ertmer, W., Birkl, G., & Lewenstein, M. (2003). Quantum computing with spatially delocalized qubits. *Physical Review Letters*, 90(14), 147901.

[4] Eckert, K., Lewenstein, M., Corbalán, R., Birkl, G., Ertmer, W., & Mompart, J. (2004). Three-level atom optics via the tunneling interaction. *Physical Review A*, 70(2), 023606.

[5] Torrontegui, E., Ibáñez, S., Modugno, M., del Campo, A., Guéry-Odelin, D., Ruschhaupt, A., Chen, X., & Muga, J. G. (2013). Shortcuts to adiabaticity. *Adv. At. Mol. Opt. Phys.*, 62, 117-169.

[6] Torrontegui, E., Martínez-Garaot, S., Ruschhaupt, A., & Muga, J. G. (2012). Shortcuts to adiabaticity: Fast-forward approach. *Physical Review A*, 86(1), 013601.

[7] Berry, M. V. (2009). Transitionless quantum driving. *Journal of Physics A: Mathematical and Theoretical*, 42(36), 365303.

[8] Chen, X., Torrontegui, E., Stefanatos, D., Li, J. S., & Muga, J. G. (2011). Optimal trajectories for efficient atomic transport without final excitation. *Physical Review A*, 84(4), 043415.

[9] Guérin, S., Thomas, S., & Jauslin, H. R. (2002). Optimization of population transfer by adiabatic passage. *Physical Review A*, 65(2), 023409.

[10] Masuda, S., & Nakamura, K. (2010). Fast-forward of adiabatic dynamics in quantum mechanics. *Proceedings of the Royal Society A: Mathematical, Physical and Engineering Science*, 466(2116), 1135-1154.

[11] Masuda, S., & Nakamura, K. (2008). Fast-forward problem in quantum mechanics. *Physical Review A*, 78(6), 062108.

[12] Masuda, S., & Nakamura, K. (2011). Acceleration of adiabatic quantum dynamics in electromagnetic fields. *Physical Review A*, 84(4), 043434.

[13] Chen, X., & Muga, J. G. (2012). Engineering of fast population transfer in three-level systems. *Physical Review A*, 86(3), 33405.

[14] Negretti, A., Benseny, A., Mompart, J., & Calarco, T. (2013). Speeding up the spatial adiabatic passage of matter waves in optical microtraps by optimal control. *Quantum Information Processing*, 12(3), 1439-1467.

[15] Sakurai, J. J, and Napolitano, J. (2010). Modern Quantum Mechanics. 2nd edition, *Addison Wesley Publishing*.

[16] Bergmann, K., Theuer, H., & Shore, B. W. (1998). Coherent population transfer among quantum states of atoms and molecules. *Reviews of Modern Physics*, 70(3), 1003.

[17] Boyer, V., Godun, R. M., Smirne, G., Cassettari, D., Chandrashekar, C. M., Deb, A. B., Laczik, Z. J., & Foot, C. J. (2006). Dynamic manipulation of Bose-Einstein condensates with a spatial light modulator. *Physical Review A*, 73(3), 031402.

[18] Fatemi, F. K., Bashkansky, M., & Dutton, Z. (2007). Dynamic high-speed spatial manipulation of cold atoms using acousto-optic and spatial light modulation. *Optics express*, 15(6), 3589-3596.

[19] Schlosser, M., Kruse, J., Gierl, C., Teichmann, S., Tichelmann, S., & Birkl, G. (2012). Fast transport, atom sample splitting and single-atom qubit supply in two-dimensional arrays of optical microtraps. *New Journal of Physics*, 14(12), 123034.

[20] Schlosser, M., Tichelmann, S., Kruse, J., & Birkl, G. (2011). Scalable architecture for quantum information processing with atoms in optical micro-structures. *Quantum Information Processing*, 10(6), 907-924.

[21] http://www.bnonlinear.com/products/112288Linear/data/112,288%20SLM%200406.pdf

[22] McGloin, D., Spalding, G. C., Melville, H., Sibbett, W., & Dholakia, K. (2003). Applications of spatial light modulators in atom optics. *Opt. Express*, 11(2), 158-166.

[23] Menchon-Enrich, R., Llobera, A., Cadarso, V. J., Mompart, J., & Ahufinger, V. (2012). Adiabatic Passage of Light in CMOS-Compatible Silicon Oxide Integrated Rib Waveguides. *Photonics Technology Letters, IEEE*, 24(7), 536-538.

[24] Longhi, S., Della Valle, G., Ornigotti, M., & Laporta, P. (2007). Coherent tunneling by adiabatic passage in an optical waveguide system. *Physical Review B*, 76(20), 201101.

[25] Bohm, D. (1952). A suggested interpretation of the quantum theory in terms of" hidden" variables. I. *Physical Review*, 85(2), 166.

[26] Oriols, X., & Mompart, J. (2012). Applied Bohmian Mechanics: From Nanoscale Systems to Cosmology. *Pan Stanford Publishing*.

[27] Benseny, A., Bagudà, J., Oriols, X., & Mompart, J. (2012). Need for relativistic corrections in the analysis of spatial adiabatic passage of matter waves. *Physical Review A*, 85(5), 053619.

[28] Nissen, A., & Kreiss, G. (2011). An Optimized Perfectly Matched Layer for the Schrödinger Equation. *Communications in Computational Physics*, 9(1), 147.

APPENDIX A
Numerical integration of the Schrödinger equation

There are many approaches to simulate the Schrödinger equation. Among them are the pseudo-spectral method, the finite element method, and the Finite Difference Time Domain (FDTD) method. In this project, we have implemented the FDTD method for solving (2.1a) and (2.1b). The main reason of choosing this method is that it is easy to be implemented and the accuracy of the simulation can be controlled easily by choosing the mesh size.

We will discuss the FDTD method for solving the time-dependent and time-independent Schrödinger equations separately.

Solving the time dependent Schrödinger equation using the FDTD method

The idea of the FDTD method is to replace the differential equation (2.1a) by a difference equation. In order to get the finite difference approximation for equation (2.1a), the Crank-Nicholson method is used. The Crank-Nicholson method can be explained as below:

Let us denote $v_i^n = v(i\Delta x, n\Delta t)$ then the Crank-Nicholson version of $\frac{\partial u}{\partial t} = F(x,t)$ is

$$\frac{u_i^{n+1} - u_i^n}{\Delta t} = \frac{1}{2}\{F_i^{n+1} + F_i^n.\} \tag{A.1}$$

If F contains derivatives with respect to space than the central difference is used in the calculation of F_i^n .

One of the problems with the FDTD or any method based on finite difference in space is the reflection from the boundary of the computation domain. This reflection is due to the Dirichlet boundary condition; that is we enforce that at the boundary the solution has to have a certain value. For example in the case of equation (2.1a), the Dirichlet boundary condition is

$$\Psi(x,t) = 0, x \in \{x_{min}, x_{max}\}, \tag{A.2}$$

with $x \in [x_{min}, x_{max}]$ being the computational domain.

Basically, there are two ways to solve this reflection problem. The first one is to get rid of the Dirichlet boundary condition and replace it by a new boundary condition called Transparent or Absorbing Boundary Condition (T/ABC) such that there will be almost no reflection at the boundaries. The second approach is to put an additional layer called the absorbing layer to absorb the coming "wave" such that, at the boundary between the layer and the non-computational domain, the reflection is negligible.

In our project we have used the second approach. The absorbing layer that we used is based on the technique called the Perfectly Matched Layer (PML) [28]. After the absorbing layer with depth, D_{PML} , is added and Dirichlet boundary condition (A.2) is applied, equation (2.1a) becomes

$$i\hbar\frac{\partial}{\partial t}\Psi(x,t) = \{\frac{-\hbar^2}{2m}\frac{1}{f(x)}\frac{\partial}{\partial x}\frac{1}{f(x)}\frac{\partial}{\partial x} + V(x,t)\}\Psi(x,t), \tag{A.3}$$

with $\Psi(x,0) = \Psi_0(x)$,
$\Psi(x,t) = 0 : x \in \{x_{min} - D_{PML}, x_{max} + D_{PML}\}$,
$V(x,t) = V(x_{min}, t) : x < x_{min}, V(x,t) = V(x_{max}, t) : x > x_{max}$,
$f(x) = 1 + e^{i\gamma}\sigma(x)$, and
$\sigma(x) = 0 : x \in \{x_{min}, x_{max}\}, \sigma(x) > 0 : x \in]x_{min}, x_{max}[$.

The value of γ used is $\frac{\pi}{4}$. This will ensure that the layer is indeed absorbing. Another point that has to be noted here is the value of $V(x,t)$ in the absorbing layer. Since the wave function in this layer is unphysical, we have some freedom in assigning the potential. The value of the potential inside can be chosen to ensure the stability of the simulation. Following the approach in [28], we have used a constant potential inside the PML layer.

Applying the Crank-Nicholson method to (A.3), we obtain the following finite difference equation

$$A_m^{\,n+1}\overrightarrow{\Psi_m^{\,n+1}} = B_m^{\,n}\overrightarrow{\Psi_m^{\,n}}, \tag{A.4}$$

where $A_m^{\,n}=[\{\frac{-ib}{2}r_m r_{m-1/2}\}\ \{1+\frac{ib}{2}r_m(r_{m+1/2}+r_{m-1/2})+\frac{i\Delta t}{2\hbar}V_m^{\,n}\}\ \{\frac{-ib}{2}r_m r_{m+1/2}\}]$

$B_m^{\,n}=[\{\frac{ib}{2}r_m r_{m-1/2}\}\ \{1-\frac{ib}{2}r_m(r_{m+1/2}+r_{m-1/2})-\frac{i\Delta t}{2\hbar}V_m^{\,n}\}\ \{\frac{ib}{2}r_m r_{m+1/2}\}]$

$r_{m\pm1/2}=\frac{r_{m\pm1}+r_m}{2,}\quad r_m=\frac{1}{1+e^{i\gamma}\sigma(m\Delta x)},\quad b=\frac{\hbar\Delta t}{2m(\Delta x)^2}$

$\overrightarrow{\Psi_m^{\,n}}=[\Psi_{m-1}^{\,n}\ \ \Psi_m^{\,n}\ \ \Psi_{m+1}^{\,n}]$

with the boundary condition and the initial condition in (A.3) applied.

Solving the time independent Schrödinger equation using the ITP + FDTD method

In order to solve equation (2.1b) using the FDTD method we incorporate the Imaginary Time Propagation (ITP) into equation (A.4). To understand the ITP method, note that the solution of (2.1a) can be written as

$$\Psi(x,t)=\sum_{n=0}^{\infty}\Phi_n(x)e^{\frac{-iE_nt}{\hbar}}, \tag{A.5}$$

where $\Phi_n(x)$ and E_n are the solutions of the eigenvalue equation (2.1b) with $E_{n+1}\geq E_n$.

By doing the transformation $t\to -it$, equation (A.5) becomes

$$\Psi(x,t)=\sum_{n=0}^{\infty}\Phi_n(x)e^{\frac{-E_nt}{\hbar}}. \tag{A.6}$$

As can be seen from equation (A.6), as *t* increases, the eigenfunctions corresponding to the excited states will die out since they will decay faster than the ground state. Hence, if we normalize the wave function at each time iteration, then we will get $\Psi(x,t)\to\Phi_0(x)$ at the end of the simulation. This is the essence of the ITP method.

In order to get the eigenfunctions of the excited states, we cancel out the spectrum of the wave function corresponded to the lower eigenvalues. That is we are doing the following step at each time iteration

$$\Psi(x,t_i)\to\Psi(x,t_i)-\sum_{n=0}^{n<N}\Phi_n(x)\int \mathrm{d}x\,\Phi_n^*(x)\Psi(x,t_i), \tag{A.7}$$

to get the N^{th} excited state. The resulting $\Psi(x,t_i)$ is then normalized. One thing to be noted is that if the eigenfunction corresponding to *N* is an odd (even) function then the initial test function should not be an even (odd) function.

The energy eigenvalue can be calculated once we obtain the eigenfunction. This is done by solving

$$E_n=\int \mathrm{d}x\,\Phi_n^*(x)H\,\Phi_n(x). \tag{A.8}$$

This equation can be easily implemented by using the central finite difference method.

It is possible to deal with the dimensionless Schrödinger equations instead of the Schrödinger equations described by (2.1a) and (2.1b). For the cases where the potential *V(x,t)* is a harmonic or a piecewise harmonic potential, the dimensionless time-dependent and time-independent Schrödinger equations can be written as

$$i\frac{\partial}{\partial t}\Psi(x,t)=\{\frac{-1}{2}\frac{\partial^2}{\partial x^2}+\frac{1}{2}x^2\}\Psi(x,t) \tag{A.9a}$$

$$E\,\Phi(x,t)=\{\frac{-1}{2}\frac{\partial^2}{\partial x^2}+\frac{1}{2}x^2\}\Phi(x,t), \tag{A.9b}$$

where the following transformation is performed in order to make the equations dimensionless

$$\begin{aligned} x &\to x\,L \\ t &\to \frac{t}{\omega} \end{aligned} \tag{A.10}$$

Particularly, after this transformation, E is expressed in units of $\hbar\omega$. In doing this transformation, it should be understood that the variables at the left side of the arrow refer to variables in equations (2.1a) and (2.1b) while the ones at the right side of the arrow are the variables in equation (A.9a) and (A.9b).

In this project, instead of solving (2.1a) and (2.1b), we solve (A.9a) and (A.9b). This is because, throughout this project, we only deal with harmonic or piecewise harmonic potentials. Note that, if we use $\hbar=\omega=m=1$, equation (A.9a) and (A.9b) are the same as (2.1a) and (2.1b), respectively. Hence the procedures described in this section can be used to solve (A.9a) and (A.9b).

APPENDIX B
Adiabaticity condition for the translation of a neutral atom in a harmonic trap

The potential of a moving harmonic trap can be written as

$$V_0(x,t)=\frac{\hbar\omega}{2L^2}(x-x_c(t))^2, \tag{B.1}$$

where $x_c(t)$ is the time-dependent position of the center of the trap. Hence, the eigenfunctions and eigenvalues can be expressed as

$$\Phi_n(x,t)=\frac{\pi^{-1/4}}{\sqrt{L}}\frac{1}{\sqrt{(2^n n!)}}e^{\frac{-(x-x_c(t))^2}{2L^2}}H_n\left(\frac{x-x_c(t)}{L}\right) \tag{B.2}$$

$$E_n=\left(n+\frac{1}{2}\right)\hbar\omega, \tag{B.3}$$

To follow the ground state adiabatically, we have to fulfill equation (2.14). In order to calculate $\langle 0;t|\frac{\partial}{\partial t}|n;t\rangle$ we use the following:

$$\langle 0;t|\frac{\partial}{\partial t}|n;t\rangle=\frac{\partial\langle 0;t|n;t\rangle}{\partial t}-\frac{\partial\langle 0;t|}{\partial t}|n;t\rangle \tag{B.4}$$

$$\begin{aligned}\frac{\partial\Phi_0(x,t)}{\partial t}&=\frac{\pi^{-1/4}}{L\sqrt{L}}\frac{\mathrm{d}x_c}{\mathrm{d}t}e^{\frac{-(x-x_c(t))^2}{2L^2}}\frac{(x-x_c(t))}{L}H_0\left(\frac{x-x_c(t)}{L}\right)\\&=\frac{\pi^{-1/4}}{2L\sqrt{L}}\frac{\mathrm{d}x_c}{\mathrm{d}t}e^{\frac{-(x-x_c(t))^2}{2L^2}}H_1\left(\frac{x-x_c(t)}{L}\right)\end{aligned} \tag{B.5}$$

$$\int_{-\infty}^{\infty}\mathrm{d}x\,H_m(x)H_n(x)e^{-x^2}=\sqrt{(\pi)}2^n n!\delta_{nm} \tag{B.6}$$

Noting that $\langle x|n;t\rangle=\Phi_n(x,t)$, and using (B.4), (B.5), and (B.6) in (2.14) we obtain

$$\left|\frac{\mathrm{d}x_c}{\mathrm{d}t}\right|\ll\frac{\omega L}{\sqrt{(2)}} \tag{B.7}$$

This expression gives the upper boundary of the speed of the trap. Our simulation results show that we can take $0.1\ll\frac{1}{\sqrt{2}}$ to be used in (B.7). Hence (B.7) can be written as

$$\left|\frac{\mathrm{d}x_c}{\mathrm{d}t}\right|\le 0.1\,\omega L \tag{B.8}$$

Equation (B.8) is used as the requirement for an adiabatic translation in this report.

APPENDIX C
Equivalence between fast-forward potential forms

Let us consider $\Psi_0(x,t)=R(x,t)e^{i\theta(x,t)}$ and $\Psi_{FF}(x,t)=R(x,\Lambda(t))e^{i(\theta(x,\Lambda(t))+f(x,t))}$. The Hamilton-Jacobi equation for $\Psi_0(x,t)$ is

$$V_0(x,t)=\frac{\hbar^2}{2m}\frac{1}{R(x,t)}\frac{\partial^2 R(x,t)}{\partial x^2}-\frac{\hbar^2}{2m}\left(\frac{\partial\theta(x,t)}{\partial x}\right)^2-\hbar\frac{\partial\theta(x,t)}{\partial t} \quad . \tag{C.1}$$

Using the Hamilton-Jacobi equation for $\Psi_{FF}(x,t)$ and taking into account the definition of $\Lambda(t)$ in [11] we obtain

$$\begin{aligned} V_{FF}(x,t) = & \frac{\hbar^2}{2m}\frac{1}{R(x,\Lambda(t))}\frac{\partial^2 R(x,\Lambda(t))}{\partial x^2} \\ & -\frac{\hbar^2}{2m}\left\{\left(\frac{\partial\theta(x,\Lambda(t))}{\partial x}\right)^2+\left(\frac{\partial f(x,t)}{\partial x}\right)^2+2\frac{\partial f(x,t)}{\partial x}\frac{\partial\theta(x,\Lambda(t))}{\partial x}\right\} \\ & -\hbar\frac{\partial f(x,t)}{\partial t}-\alpha(t)\hbar\frac{\partial\theta(x,t')}{\partial t'}\Big|_{t'=\Lambda(t)} \quad . \end{aligned} \tag{C.2}$$

By inserting (C.1) to (C.2), we obtain

$$\begin{aligned} V_{FF}(x,t) = & \alpha(t)V_0(x,\Lambda(t)) \\ & +(\alpha(t)-1)\frac{\hbar^2}{2m}\left\{-\frac{1}{R(x,\Lambda(t))}\frac{\partial^2 R(x,\Lambda(t))}{\partial x^2}+\left(\frac{\partial\theta(x,\Lambda(t))}{\partial x}\right)^2\right\} \\ & -\frac{\hbar^2}{2m}\left\{\left(\frac{\partial f(x,t)}{\partial x}\right)^2+2\frac{\partial f(x,t)}{\partial x}\frac{\partial\theta(x,\Lambda(t))}{\partial x}\right\}-\hbar\frac{\partial f(x,t)}{\partial t} \quad . \end{aligned} \tag{C.3}$$

Next, we use the following identities

$$\Re\left(\frac{1}{\Psi_0(x,t)}\frac{\partial^2\Psi_0(x,t)}{\partial x^2}\right)=\frac{1}{R(x,t)}\frac{\partial^2 R(x,t)}{\partial x^2}-\left(\frac{\partial\theta(x,t)}{\partial x}\right)^2 \tag{C.4a}$$

$$\Re\left(i\frac{1}{\Psi_0(x,t)}\frac{\partial\Psi_0(x,t)}{\partial x}\right)=-\frac{\partial\theta(x,t)}{\partial x} \tag{C.4b}$$

to get

$$\begin{aligned} V_{FF}(x,t) = & \alpha(t)V_0(x,\Lambda(t))-(\alpha(t)-1)\frac{\hbar^2}{2m}\Re\left(\frac{1}{\Psi_0(x,\Lambda(t))}\frac{\partial^2\Psi_0(x,\Lambda(t))}{\partial x^2}\right) \\ & +\frac{\hbar^2}{2m}\Re\left(2i\frac{\partial f(x,t)}{\partial x}\frac{1}{\Psi_0(x,\Lambda(t))}\frac{\partial\Psi_0(x,\Lambda(t))}{\partial x}\right) \\ & -\frac{\hbar^2}{2m}\left(\frac{\partial f(x,t)}{\partial x}\right)^2-\hbar\frac{\partial f(x,t)}{\partial t} \end{aligned} \tag{C.5}$$

which is the form of $V_{FF}(x,t)$ in [11].

To get the expression for $f(x,t)$, we can use the continuity equation for $\Psi_0(x,t)$ and $\Psi_{FF}(x,t)$. This has been explained in [11]. The result is

$$\frac{\partial f(x,t)}{\partial x}=(\alpha(t)-1)\frac{\partial\theta(x,\Lambda(t))}{\partial x} \quad . \tag{C.6}$$

One obvious solution for $f(x,t)$ is

$$f(x,t)=(\alpha(t)-1)\theta(x,\Lambda(t)) \quad . \tag{C.7}$$

By inserting (C.7) to (C.2) and using (C.1) to replace $\frac{1}{R(x,\Lambda(t))}\frac{\partial^2 R(x,\Lambda(t))}{\partial x^2}$ in (C.2), we

obtain

$$V_{FF}(x,t)=V_0(x,\Lambda(t))-\hbar\theta(x,\Lambda(t))\frac{\partial\alpha}{\partial t} \\ -(\alpha^2(t)-1)\{\hbar\frac{\partial\theta(x,t')}{\partial t'}|_{t'=\Lambda(t)}+\frac{\hbar^2}{2m}(\frac{\partial\theta(x,\Lambda(t))}{\partial x})^2\}. \quad (C.8)$$

which is equation (3.5) in Section 3.1.1.

Fast-Forward Potential in Shortcut to Adiabaticity: A misleading route

Here we will show that it is important to avoid a misleading route to obtain the shortcut to adiabaticity using the Fast-Forward technique. In this misleading route, instead of equation (3.5), we will start with equation (3.6). Except at the position where $\phi(x_a,t)=0$ and $\lim_{x\to x_a^-} sgn(\phi(x,t))\neq\lim_{x\to x_a^+} sgn(\phi(x,t))$, we can write

$$\frac{-\hbar^2}{2m}\frac{1}{R(x,t)}\frac{\partial^2R(x,t)}{\partial x^2}+V_0(x,t)=\frac{-\hbar^2}{2m}\frac{1}{\phi(x,t)}\frac{\partial^2\phi(x,t)}{\partial x^2}+V_0(x,t)=E(t)\ . \quad (C.9)$$

Using (C.9) in (3.6) and ignoring space-independent terms we obtain

$$V_{FF}(x,t)=V_0(x,\Lambda(t))-\hbar\delta(x,\Lambda(t))\frac{\partial(\alpha\epsilon)}{\partial t}\ . \quad (C.10)$$

The expression of $V_{FF}(x,t)$ in (C.10) is simpler than equation (2.28) in [10] and it is also simpler than equation (3.5) in Chapter 3. Nevertheless, there is one problem in the derivation above. We have assumed that $\Psi_0(x,t)\approx|\phi(x,t)|e^{i\theta(x,t)}$ can be used. In this way, we can obtain (C.9). However, this assumption can not be used to calculate $\frac{-\hbar^2}{2m}\frac{1}{R(x,t)}\frac{\partial^2R(x,t)}{\partial x^2}+V_0(x,t)$ such that it is correct within the order of $O(\epsilon^2)$. Hence it can not be used in (3.6).

Note that in deriving equation (3.6) we have used the Hamilton-Jacobi equation to replace $\{\hbar\frac{\partial\theta}{\partial t}|_{\Lambda(t)}+\frac{\hbar^2}{2m}(\frac{\partial\theta(x,\Lambda(t))}{\partial x})^2\}$ in (3.5) with $\frac{-\hbar^2}{2m}\frac{1}{R(x,t)}\frac{\partial^2R(x,t)}{\partial x^2}+V_0(x,t)$. The failure of using $\Psi_0(x,t)\approx|\phi(x,t)|e^{i\theta(x,t)}$ in calculating $\frac{-\hbar^2}{2m}\frac{1}{R(x,t)}\frac{\partial^2R(x,t)}{\partial x^2}+V_0(x,t)$ means that there should be a contradiction when we use $\Psi_0(x,t)\approx|\phi(x,t)|e^{i\theta(x,t)}$ in both the continuity equation and the Hamilton-Jacobi equation.

Here we give one example of such a contradiction based on equation (3.32). There, the space-dependent component of the phase of the wave function in the case of adiabatic translation of a single neutral atom is calculated. Using (3.32) in the Hamilton-Jacobi equation gives

$$\frac{-\hbar^2}{2m}\frac{1}{R(x,t)}\frac{\partial^2R(x,t)}{\partial x^2}+V_0(x,t)=\hbar\frac{\partial\delta}{\partial t}+\frac{\hbar^2}{2m}(\frac{\partial\delta(x,t)}{\partial x})^2+g(t) \\ =mxT_0\frac{d^2x_c}{dt^2}+\frac{m}{2}(T_0\frac{dx_c}{dt})^2+g(t) \quad (C.11) \\ =mxT_0\frac{d^2x_c}{dt^2}+g_2(t).$$

Equation (C.11) shows that $\frac{-\hbar^2}{2m}\frac{1}{R(x,t)}\frac{\partial^2R(x,t)}{\partial x^2}+V_0(x,t)$ has a space-dependent term. However, equation (C.9) does not. Hence, the contradiction.